Southern Hemisphere Monsoonal System during Superinterglacial Stages: MIS5e, MIS11c and MIS31

Carlos Diego Gurjão (carlosdiegogurjao@gmail.com)
Federal University of Vicosa: Universidade Federal de Vicosa https://orcid.org/0000-0001-5496-7418
Flávio Justino
Federal University of Vicosa: Universidade Federal de Vicosa
Gabrielle Pires
Federal University of Vicosa: Universidade Federal de Vicosa
Mônica Senna
UFF: Universidade Federal Fluminense
Douglas Lindemann
Federal University of Pelotas: Universidade Federal de Pelotas
Jackson Rodrigues
UFF: Universidade Federal Fluminense

Research Article

Keywords: Climate changes, Sea Surface Temperature, Interglacials, Marine Isotope Stages

Posted Date: May 5th, 2022

DOI: https://doi.org/10.21203/rs.3.rs-1617908/v1

Noname manuscript No.
(will be inserted by the editor)

Southern Hemisphere Monsoonal System during Superinterglacial Stages: MIS5e, MIS11c and MIS31

Carlos Gurjão · Flávio Justino · Gabrielle Pires · Mônica Senna · Douglas Lindemann · Jackson Rodrigues

Received: date / Accepted: date

Abstract Based on coupled climate experiments conducted with the coupled ICTP-CGCM model focusing on interglacial stages MIS5e (127 ka), MIS11c (409 ka) and MIS31 (1,072 ka), the Austral summer monsoonal system is investigated. The interannual variability and intensity of monsoon events are analysed from vorticity indices and air-sea interaction processes for Africa, Australia and South America monsoons. Results demonstrated with respect to present day conditions, an orbital driven decrease in precipitation in summer, but slightly shift of the onset and demise periods of monsoons. Sensitivity experiments indicate, furthermore, that the monsoons are forced not only by external factors such as the dominant effect of insolation, but also by distant climate anomalies, such as surface temperature of the equatorial Atlantic and Pacific basins. During the interglacial stages, cooling occurs in the Southern Hemisphere whereas Northern Hemisphere substantially warms, inducing remarkable changes in the position of the oceanic subtropical high pressure systems and equatorial convergence zone. Regionally, these mechanisms contribute to periods of drought, with reduced precipitation rate over sectors of the Amazon and Northeastern Brazil, northern Australia and southern Africa. Monsoonal rainfall shows different responses to precessional forcing, as well as the relationship between the monsoon and Niño 3.4 differs among the interglacial stages. Compared to current climate, correlation

Carlos Diego de Sousa Gurjão
Federal University of Viçosa
Department of Agricultural Engineering
E-mail: carlosdiegogurjao@gmail.com

Flávio Justino
Federal University of Viçosa
Department of Agricultural Engineering

analyses have demonstrated weaker influence of the equatorial Pacific Ocean on the Austral summer monsoon for the MIS5e, MIS11c and MIS31. Exception is noticed for the South America monsoon, where the Niño 3.4 exerts a more prominent role in these distant intervals, in consonance with the tropical Atlantic in particular during the MIS5e.

Keywords Climate changes · Sea Surface Temperature · Interglacials · Marine Isotope Stages

1 Introduction

Modelling studies that investigate the impact of changes in seasonality on global heat content provide an opportunity to understand past and future climate features, in particular the monsoonal system, which is highly dependent on surface thermal conditions (Diaz and Boos, 2021; Zeng and Zhang, 2020; Deng et al., 2018; Yin and Berger, 2012). Global precipitation is primarily dominated by summer monsoon characteristics, which have been found to be highly correlated with the annual cycle of solar insolation, as well as associated with changes in radiative forcing due to increased greenhouse gases (Geen et al., 2020; Li and Ting, 2017; Trenberth et al., 2000). Studies have demonstrated that global hydrological cycle becomes stronger in a warmer climate (Held and Soden, 2006), but additional scrutiny is needed to verify hydroclimatic changes under precessional inter-hemispheric seesaw temperature anomalies; with warmer Boreal latitudes and Austral cooling, as characteristics of interglacial stages (Justino et al., 2017; Melles et al., 2012; Braconnot et al., 2008; Lisiecki and Raymo, 2005). Indeed, past changes in the radiative forcing have been responsible for weakening the SH monsoons in the mid-Holocene as a result of decreased net energy input (D'Agostino et al., 2020).

Among interglacial stages, the Marine Isotope Stages (MIS) MIS5e (127 ka), MIS11c (409,000 ka) and MIS31 (1072 ka), for instance, are marked by Northern Hemispheric increases in summer oceanic and terrestrial temperatures. The MIS5e also knows as the Eemian, experienced sudden changes in the dynamics of the atmosphere and ocean in response to strong insolation in the Northern Hemisphere (NH) but weaker in the Southern Hemisphere(SH) (Yin and Berger, 2012; Berger and Loutre, 1991; Members, 2006; Siccha et al., 2015; Bard et al., 1990). Additional findings also indicate that the northward migration of the Intertropical Convergence Zone (ITCZ) during the Eemian, favored more intense NH summer monsoon with respect to the present climate (Montoya et al., 2000) .

The MIS11c ($\sim$ 409 ka BP) also experienced global high temperatures dictated by increases in Boreal insolation. However, the Asian summer monsoon (ASM) during MIS11c, as revealed by data from the Yongxing cave, China, does not differ remarkably from monsoon characteristics in the Late Holocene (Zhao et al., 2019). It should be noted that the intensity of the MIS11c warming, is regionally dependent (Yin and Berger, 2012; Oppo et al., 1998; Rousseau et al., 1992), raising questioning on how MIS11c warming or slight cooling may have induced changes in local precipitation features. For instance, the East Asian summer monsoon (EASM) responds differently to strong summer insolation during the MIS13, contributing to strengthen significantly the summer precipitation in northern China but barely changing that in southern China (Yin et al., 2014). Additional effort might indeed be pursued to clarify these issues based on coupled modelling experiments, carried under drastically modified astronomical forcing.

The MIS31 represents one of the last interglacials ever recorded, being considered the warmest marine isotope stage interval that contributed to substantial melting of NH polar glaciers compared to the present day (Lisiecki and Raymo, 2005; Melles et al., 2012). Such changes also impacted the seasonality of NH atmospheric and oceanic circulation patterns, and El NIÑO Southern Oscillation (ENSO) intensification and periodicity, besides significant changes in the Meridional Overturning Circulation (MOC). Insofar as monsoonal patterns are concerned, it is found that the Indian monsoon was enhanced but no correlation with the ENSO is identified in the MIS31 climate, differing from conditions delivered by today's climate. It has also been found that monsoonal precipitation for this interglacial is more closely connected to hemispherical features than to the tropical–extratropical climate interaction (Justino et al., 2019). Oliveira et al. (2017) argue that low-latitude insolation forcing plays an important role during the MIS31 by inducing a mild and humid climate regime in the Mediterranean region, with reduced seasonality.

Despite large effort in characterizing in detail those past climatic features, the spatio-temporal patterns of SH monsoon related to changes in external factors is urgent needed. These monsoon characteristics are more noticeable during the austral summer, in which the inversion of the zonal wind component from east to west are highly correlated to significant increases in precipitation rates (Yim et al., 2014; Geen et al., 2020). The seasonal zonal wind shifts in the lower troposphere is a response to the thermal contrast between ocean and continent, which causes rainy summers and dry winters. Moroever, in some locations monsoonal precipitation is associated with climatic extremes, because leads to flash floods and notorious damage to the population, especially to most vulnerable people, in urban and agricultural zones (Ávila Díaz et al., 2016; Kundzewicz et al., 2014). The weakening of the monsoon on the other hand leads to the absence of water resources and extreme heat during drought events (Deng et al., 2018; Ha et al., 2020). It is worth noting that most of agricultural activities in South America, Africa and Australia are highly dependent on monsoonal driven-precipitation. Therefore, investigation of the SH monsoon system under very different climates, as delivered during past interglacial, are very useful to foresee adaptative measures to cope with future changes in the anthropocene.

Thus, past interglacial temperature contrasts between land and oceanic regions, and the out-of-phase Sea Surface Temperature (SST) pattern induced by the precessional cycle, between the Northern and Southern Hemispheres might have dictated remarkable changes in seasonal precipitation. The SH monsoon is evaluated here based on a series of coupled climate model simulations conducted for different interglacial stages, including all forcing factors such as changes in orbital parameters and greenhouse gases characteristics of the epoch. In section 2 is describe the coupled model specifications and experimental modelling setup. Section 3 discuss results under different perspectives: (1) the control climate is compared to ERA5, (2) changes in the radiative components and temperature are analysed; and (3) the impact of those changes on atmospheric dynamics responsible for anomalous magnitude, onset and cessation of monsoonal precipitation during the interglacials, are shown. In session 4, conclusions are summarised in the light of previous investigations and paleo-proxies perspectives.

2 ICTP-CGCM and modeling experiment design

The present study applies the Global Coupled Atmosphere-Ocean Circulation Model developed at the International Centre for Theoretical Physics (ICTP-CGCM), which consists of the global atmospheric climate model "SPEEDY" (version 41) coupled to the Nucleus for European Modeling of the Ocean (NEMO) model (Madec et al., 1998; Madec, 2008), with the coupler OASIS3 (Valcke, 2013). In computational terms, SPEEDY proofs to be effective in reproducing the main characteristics of the climate system of tropical and extratropical latitudes (Molteni, 2003; Kucharski et al., 2006; Justino et al., 2021). The atmospheric component runs at eight vertical levels in T30 horizontal resolution (Kucharski et al., 2016). NEMO is an ocean model adapted for regional and global ocean circulation studies, based on 31 vertical levels with thicknesses ranging from 10 to 5000 meters of the ocean floor, with 16 levels in the first 200 meters. The current version uses a tri-polar ORCA2 configuration with a horizontal grid resolution of 2° and a tropical refinement of 0.5° (Madec, 2012).

To investigate interglacial intervals three experiments integrated from 500 years after the spin-up were carried out (Table 1). Greenhouse gas concentrations, as well as the orbital parameters have been set according to Coletti et al. (2015); Bereiter et al. (2015); Lüthi et al. (2008). The study centered the interglacial time at three fixed periods, 127 ka (MIS5e), 409 ka (MIS11c) and 1,080 Ma (MIS31), for this reason, the orbital forcing is characteristics of the vernal equinox as the control experiment (CTRL) climate. The CTRL is conducted under current orbital forcing and atmospheric conditions as described in (Justino et al., 2017, 2019). For all experiments the first 100 years of the simulation are not included in the analyses of results. Verification of the CTRL climate in reproducing present day conditions is based on comparison with the ERA5 database (Hersbach, 2016) from 1979 to 2020, insofar as characteristics of the tropical climatology of precipitation, zonal component (u), SST and Sea Level Pressure (SLP) are concerned.

3 Results

3.1 **Differences between the CTRL simulation and MIS experiments**

3.1.1 ***CTRL radiative components and temperature***

Based on Table 1, it is noticed that no remarkable changes of the atmospheric composition exist among the interglacials, but they favour slightly cooling conditions with respect to CTRL, due to lower atmospheric CO_2 concentration and weaker greenhouse capacity of the atmosphere, during those past interglacial. These features contrast with modifications of the Earth's orbit, in particular the precessional cycle. Largest differences with respect to CTRL are noticed in the MIS31 resulting in very distinct climate (Justino et al., 2021; Coletti et al., 2015). Figure 1 shows zonally averaged radiative components at the top of atmosphere (TOA) based on ERA5 and the CTRL simulation. This is important because main differences between the MIS experiments and CTRL primarily derives from changes in the radiative forcing. Thus, verifying the ICTP-CGCM capability to reproduce ERA5 demonstrates whether the model is suitable for the proposed investigation.

Overall, the coupled model is able to represent the energy balance at the TOA and surface. However, the ICTP-CGCM underestimates ERA5 values about by 5% at the TOA (Fig. 1a). Good match between ERA5 and the model is found in the zonal distribution, but the presence of the Intertropical Convergence Zone (ITCZ) in the equatorial region, leads to more pronounced differences across 10°S and 10°N. Atmospheric models running under lower resolution show drawbacks in reproducing meso-scale convective system in the tropics leading to slightly modified radiative balance. In the polar regions and extratropics as expected (Fig. fig1a), more energy is emitted to space via longwave radiation than is provided by the shortwave component. In general grounds, the modelled radiative budget (Rn) is well represented by assuming the meridional gradient of the radiative components, that in fact, is responsable for the large-scale atmospheric and oceanic circulations. It should be emphasised that estimates of the radiative balance has been for many years a challenging task associated with improvements of coupled models (Wild, 2020).

Figure 1b,c,d show differences of the short wave radiation at the top of the atmosphere, during the interglacials MIS5e, MIS11c and MIS31 with respect the CTRL climate. The influence of modified orbital parameters leads from June to November in the SH tropics, to an increase of 60 Wm^{-2} in the MIS5e and 20 Wm^{-2} in MIS11c (Fig. 1b-c). The most significant increase is, however, observed in NH where the shortwave radiation is larger than CTRL in summer and extends throughout the hemisphere. The MIS31 is among the interglacial periods the most affected by orbital changes from March to October. It should be stressed that from November to March, the SH experiences a drop in the amount of incoming energy, from October to February, which is the dominant period of the monsoonal features (Fig. 1b-d). This reveals that the general attribution for warmer climates in past interglacial should be taken in light of individual hemispheres and seasonal dependence.

Figure 2 shows that modified orbital parameters and subsequent changes of incident solar radiation result in anomalous near surface air temperatures. Differences during the interglacials with respect to current climate, are characterized by cooling from November to February (NDJF) across the continents (Fig. 2a-c-e). This gradually turns to warmer conditions in Boreal spring with largest anomalies found in summer, which are reproduced by annual mean anomalies (Fig. 2b-d-f). The SH summer monsoons, which are dominant in NDJF months, can be severely affected by surface thermal changes not only causing a reduction in the amount of rainfall, but also by inducing distinct onset and demise periods. Surface condition are determinant for SH monsoons because soil moisture and evapotranspiration play an important role at early stages of the monsoon (Collini et al., 2008). In particular, when water vapour advection from surrounded monsoonal domain is weak. Indeed, lower temperatures are also a consequence of reduce energy and evaporation from the surface, causing a weakening in the convection of the monsoon system (D'Agostino et al., 2020).

These changes across the tropical region, which is an important source of humidity to the subtropics, can directly impact monsoonal characteristics. The substantial warming delivered over the continents as shown by annual time averaged (Fig. 2b-f), induces a northward migration of the ITCZ, as well as a weakening of the southern trade winds (Justino et al., 2019). It is not speculative to argue that these anomalous features will be associated with modifications in the thermal ocean-land characteristics, impacting the monsoonal system.

3.1.2 ***Annual distribution of precipitation and the SH monsoonal characteristics***

To identify the SH monsoons spatial domain, the amplitude of the first harmonic of precipitation has been applied (Fig.3a,b). The first harmonic characterizes regions where the annual cycle is dominant explaining more than 80% of the variance. This fits nicely with monsoonal features. Figure 3a depicts the first harmonic amplitude of precipitation from the 12 months climatology, based on a 100-year CTRL simulation. Harmonic analyses also known as Fourier transformation, are computed on a series of sine and cosine functions which may be used to verify differences in the precipitation magnitude between the rainy and dry seasons, for instance. When the seasonal cycle is dominant, the 1st harmonic explains most of the variance, which is the case in monsoonal regions. The ICTP-CGCM is capable to reasonable simulate the amplitude over the South African Monsoon System (SAFMS), the Australian Monsoon System (AUSMS) and the South American Monsoon System (SAMS) regions (Fig. 3a). The CTRL experiment (Fig. 3b), however, overestimates the 1st harmonic amplitudes by 5 mm/day in particular across SAMS, in comparison to values delivered by ERA5 dataset (Fig.3a,b). Drawbacks in simulating tropical dynamics in coupled models, arise due to limitations in reproducing ocean-atmosphere interaction, as compared to processes in the extratropics, because based on intermediate complexity atmospheric components, convection, turbulent heat fluxes and diabatic processes are more difficult to be parameterized (Flato et al., 2014; Neelin et al., 1994). Marengo et al. (2012)

Furthermore, it should be mentioned that the CTRL climate discussed here shows differences from ERA5, in part because time intervals used are not the case. The CTRL is based on a 100 years simulation forced with initial conditions correspondent to 1950. Certainly, these different intervals drive slightly distinct climates, also due to the ICTP-CGCM interannual and interdecadal variability, which may differ with respect to ERA5 conditions computed from 1979 to 2020.

The SH monsoonal regions, present a well-defined annual cycle, with rainy summers (DJFM) and dry winters (MJJA), as shown in Figure 3c-d-e. The CTRL climate delivers with respect to ERA5, higher precipitation as reproduced by areal averages over SAMS and AUSMS but lower values are found for SAFMS. Among the monsoons, higher daily precipitation amount is delivered for the AUSMS ($\approx$ 10 mm/day), whereas lower values are observed in the SAFMS ($\approx$ 6 mm/day), during the peak month.

This is highlighted from November to March. Regionally, 70% of annual rainfall occurs during the NDJF months related to the monsoons. ERA5 shows along the SAMS, SAFMS and AUSMS domains, magnitudes by about 7, 9 and 8 mm/day (Fig. 3c-e).

Correlation analyses show reasonable correspondence between ERA5 and the CTRL run (Table 2), based on monsoon indices as represented by the zonal circulation and the areal averaged rainfall, values up to 0.93 and 0.74 are found for AUSMS and SAFMS, but much lower is delivered for SAMS. This indicates that insofar as the SAMS is concerned, the vorticity index in the CTRL run is not able to individually represent precipitation changes related to the monsoon. The presence of the Andes, the recurrent cold fronts and the Amazonian contribution to the SAMS through evapotranspiration, are complex features that may weak the correlation between the vorticity index and SAMS precipitation. It may be argue that nearby oceanic processes exert an important role to define the SAM. These processes involve SST changes in the southwestern Atlantic Ocean, which impact in two-ways interaction the strength of the South Atlantic Convergence Zone (SACZ), by modifying the maritime water vapor and heat transports onto continental regions (Pezzi et al., 2022; Jorgetti et al., 2014). The SST impact on the monsoonal system is discussed in more detail in the following sections.

3.1.3 ***Monsoonal precipitation***

In the interglacial experiments, changes in insolation during the interglacial lead to drastically modified monsoonal precipitation amounts (Fig. 4). Precipitation anomalies related with interglacial periods (Fig. 4a-f) deliver distinct pattern associated to each monsoon domain. Results show that increased precipitation occurs in the dry season (June, July and August) in particular for SAMS and SAFMS (Fig. 4c,f). These features are enhanced in the MIS11c and MIS5e, and may represent a slightly shift in the rainy period over the two monsoons domains. In AUSMS, larger changes are depicted from October to February, with a drop in rainfall (Fig. 4e), however, therefrom there exist an enhancement of the monsoonal precipitation until April. The interglacial driven by strongest orbital radiative forcing, the MIS31, delivers remarkable changes with respect to the CTRL, with substantial reduction of precipitation in the SAMS, by more than 60% (Fig. 4f). Reduction is also found for the other SH systems, the weakening of the SAFMS precipitation occurs during the summer months, whereas for the AUSMS drier conditions are found from June to December with respect to the CTRL climate (Fig. 4d,e).

Changes in surface conditions such as shown by evapotranspiration (ET, Fig. 4g-i) in line with those depicted by precipitation in the SAFMS, indicating the importance of interaction between surface processes and precipitation, in particular soil moisture. Analyses for the other two SH monsoon do not demonstrate a close relationship between ET and precipitation. In the AUSMS, enhanced monsoon rainfall is accompanied by reduced ET, which lead to assume that the AUSMS during these interglacial, experiences large contribution from water vapor transport originating from outside the monsoonal domain. The pattern over the SAMS shows a time lag relationship, in which the peak in reduction of ET leads by two months negative anomalies of precipitation in the MIS11c and MIS5e. In the case of MIS31, changes in ET seems to influence in lower degree modification of precipitation, with respect to the other interglacials (Fig. 4g-i).

The Hovmöller diagram (Fig. 5) based on the 850hPa zonal wind shows onset and demise of the rainy season related to the monsoon, through the inversion of the zonal wind; eastward winds in the dry season and westward winds more dominant for the rainy season. In general, changes in atmospheric circulation via the inversion of the zonal wind are well simulated by the ICTP-CGCM (Fig. 5a-b-c). In terms of individual monsoons, close pattern is depicted for the SAFMS and AUSMS, by indicating an east-west wind shift during the summer months (Fig. 5a-b). A different pattern emerges for the SAMS, where wind transition is not clearly seen. However, in the SAMS wind features are longitudinal depend, and confined to the eastbound of the monsoon from 60°-30°W(Fig. 5c). Despite reasonably reproducing the monsoon annual cycle, the ICTP-CGCM does not relate the wind features to precipitation in the SAMS domain. This is associated with the topographic barrier imposed by the Andes, which channels throughout the year the easterly Atlantic flow, hampering the seasonal shift, as discussed by Nogués-Paegle et al. (2002).

The MIS5e and MIS11c deliver a semi-annual component that is most evident in the AUSMS domain. This characteristic found in the SAFMS and AUSMS, is absent in the MIS31, which exhibits a well defined annual cycle (Fig. 5j,k). Indeed, stronger annual cycle in the MIS31 has been found by Justino et al. (2019). Weaker interannual ENSO may acts in line to enhance the orbital forcing. The SAMS is different because it experiences large changes related to the implementation of the orbital forcing (Fig. 5f,i,j). For this monsoon, the MIS5e and 11C differ substantially from the CRTL with increased zonal wind shear, and subsequently increased convergence over 45°W, from December to March (Fig. 5j,i). Moreover, it is found drastically modified circulation from August to November, with respect to CTRL. Strong westerly flow is evident in the MIS5e and MIS11c climates from 60-30°W. This results from intensified sub-tropical Atlantic high.

In order to evaluate in more detail mechanisms responsible for interglacial monsoonal changes, it is shown in Figure 6, the correlation pattern between the SAFMS, AUSMS and SAMS vorticity indices and SST changes. It highlights that similarities between the SAFMS and AUSMS under CTRL conditions, do not propagate through interglacials stages (Fig. 6a-h). The MIS5e exhibits a pattern, in particular across the Pacific Ocean, that is between CTRL and the other more distant interglacials, MIS11c and MIS31. For instances, both monsoon seem to be well correlated with Pacific and Indian Ocean SST in the CTRL climate, however, in MIS11c and MIS31, the SAFMS is highly related to Indian Ocean only (Fig. 6c,d). In the AUSMS case, changes over the warm pool Pacific region are dominant insofar as SST are concerned because weak correlation are found over the NIÑO (Equatorial Pacific) region (Figs. 6g,h).

As demonstrated by previous discussion, the SAMS (Fig. 6i-l) differs substantially from the other monsoons. The Atlantic Ocean exerts an important role which is dependent upon the interglacial investigated. Indeed, in CTRL conditions higher positive correlations are found between precipitation and warmer Atlantic SST, under La Niña-like background (Fig. 6i). Turning to MIS5e, the presence of the Atlantic variability (TAV, (Cabos et al., 2019) is enhanced with respect to CTRL, with a well defined dipole (Fig. 6j).

This SST correlation pattern indicates a southward position of the ITCZ, due to northern Atlantic cooling. Positive correlation also in the southwestern Atlantic is other feature that indicates intensification of the ZCAS. The relationship between SST and SAMS precipitation for the MIS11c and MIS31 demonstrated that the positive correlation is weaker in the equatorial southern Atlantic in the MIS11C, whereas an overall anticorrelation is found in the MIS31 (Fig. 6i). In general, the MIS31 exhibits contrasting values with respect to the CTRL (Fig. 6i,l), insofar as the SAM is concerned.

The eastern tropical Pacific exhibits a strong relationship with continental tropical rainfall, particularly due to ENSO characteristics. Table 3 indicates that during El NIÑO events, monsoonal precipitation of the three analyzed sectors is reduced with larger changes for AUSM in both ERA5 and in CTRL. These significant correlations, however significant, also reveal that NINO34 can drive interannual variability over the summer monsoons for the MIS5e and MIS11c, with exception of the AUSSM sector. On the other hand, the AUSSM is negatively correlated with ENSO in MIS31 at a 95% confidence level.

Although, the spatio-temporal variability patterns of rainfall are different for each interglacial, it depends on the intensity of individual ENSO events. Because NINO34 may be projected as a remote forcing, it changes local thermodynamic and dynamic processes influencing climate and weather at long distances (McPhaden et al., 2006).

Also in this study, we examined the correlations between SH continental monsoon rainfall and Tropical Atlantic Variability (TAV). Under CTRL conditions most correlations are not significant. Turning yo the interglacial behavior, the analyses demonstrate correlations are weaker with respect to ENSO, but significant over the SAMS in the MIS5e. Interesting is that correlations between TAV and SAMS (-0.33) are higher than correlations based on ENSO (-0.29) (Table 3).

3.1.4 ***Spatial patterns of Precipitation and SLP***

Figures 7 and 8 show differences in precipitation and SLP (interglacial minus control) overlaid with significant correlation (dotted) between the regional monsoon vorticity index; and precipitation and SLP. Analyses of SLP are important because may indicate regions of low and high pressure systems within monsoon domains in the lower troposphere. This can be further used to find convergence and divergent flows, which may induce or suppress precipitation.

During the DJFM season for MIS5e and MIS11c, there was a reduction in rainfall in southern/southeast Africa and much of South America with values from -2 to -5 mm/da (7(a-f), with respect to CTRL. Precipitation increases are found in the Indonesian Archipelago and southern Australia by up to 4 mm/day (Fig. 7(b-e)). The dominant effect of the orbital forcing in all 3 interglacial is highlighted as reduced precipitation across most of continental regions. In the MIS31, reduced rainfall in Africa and South America show values between -2 mm/day and -6 mm/day (Fig. 7g-i). Rainfall increases in northern Amazon and semiarid Northeast Brazil (3 mm/day), but there is no evidence that this is linked to monsoonal changes. It should be noted that precipitation changes in Australia are lesser affected by the implementation of the orbital forcing. Most anomalies range between ± 2 mm/day, and in the MIS31, are not statistically significant.

Analyses of differences of SLP may clarify causes of precipitation changes. The SLP anomalies between the interglacials experiments (MIS5e, MIS11c e MIS31) and CTRL, exhibit statistically significant increased pressure in line with precipitation reduction over SAFMS, AUSMS and SAMS regions (Figures 8). Differences of MIS11c and CTRL, on the other hand, show slight reduction in SLP across southern Australia and south-central Brazil (Figures 8e,f). Those low pressure anomalies induce precipitation (Fig. 7) in Australia by enhancing convection and upward motion. It has to be noticed that this drop in SLP during the MIS11c in southern Brazil/South America, theoretically would increase the frequency of subtropical frontal systems, passing onto the SAMS region, but the high pressure anomaly associated with the subtropical Atlantic high, leads to a blocking situation hampering the subtropical system to move northwards. Thus, leading to dryness in most of Brazil during the interglacial. In the MIS31, most striking feature is related to cooling in the western Pacific by up to -3°C, in particular over the AUSMS domain. This results in positive SLP anomalies characteristics of permanent El NIÑO conditions (Fig. 2c,e and 8h), and reduced monsoonal precipitation (Fig. 7h).

3.1.5 ***Intercomparison between modeled precipitation and proxies data***

Paleoclimate simulations are able to simulate Earth's climate in distant past, but comparison with reconstruction are still necessary to reveal model-proxies differences, in regions where models may struggle to represent particular atmospheric/oceanic features. Thus, indicating climate mechanisms that should be addressed in more detail (Braconnot et al., 2012). Justino et al. (2017) provides an evaluation of modeled MIS31 surface temperature and proxies, in which demonstrated that the ICTP-CGCM is able to reproduce reconstructions, differing only by ± 1°C, but larger values up to 3°C are found in the extratropics. These large differences have been attributed to reduced NH seaice cover, and therefore higher SSTs.

The three interglacials are warmer (colder) in the NH (SH) than the CTRL climate (Table 4). This seesaw feature is related to changes in the magnitude of seasonal insolation. It is also worth mentioning that the ICTP-CGCM model simulates lower temperatures than reconstructins primarily in the Austral extratropical region for the MIS5e and MIS11c. On the other hand, these two interglacials show warmer temperatures in the NH (2-6$^{\circ}C$). This peculiar warming in the NH during MIS5e and MIS11c may indicate the model characteristics in reproducing the seaice extent, highlighted by increased cover in the SH but widespread reductions in sea ice across the NH. These changes in high latitudes are able to modify the meridional thermal contrast, impacting the atmospheric circulation and local turbulent oceanic fluxes, which can result in distinct SSTs.

Reconstruction also exhibits caveats because in some cases they may reproduce long term changes that are dictated by a particular seasonal strength, such as demonstrated by Liu et al. (2014). This argumentation is not used to justify differences between model and reconstructions, but usefully serves to indicate that reconstruction represent local conditions that can be smoother in a grid box representation. Hydroclimatic reconstructions from MIS5e and MIS11c are shown in Table 5 and Figure 9, across the 5°N-33° domain. This allows to identifying the precipitation and evaporation relationship, and therefore atmospheric humidity in both time slices, with respect to CTRL climate. By evaluating proxies for individual latitudinal bands divided by $10\circ$ shows that between $5\circ$N-$5\circ$S, drier conditions prevailed during NDJF months in the MIS5e, with exception of African sites in reconstruction and model results (red circles in Fig. 9). These conditions are present not only during the monsoonal season bit it is distributed throughout the year (Fig. 9a,b,c).

From 6°S to 15°S most reconstructions are marked by increased humidity (blue circles in Fig. 9, differing from simulated values, that during the monsoons show dryer conditions, in particular in central Africa and Australia. Agreement is found over Indonesian Archipelago, east Africa and the Andes. However, by comparing reconstructions and model results, good agreement between these data is found for the MAMJ and JASO months, which indicates that reconstructions primary reproduce enhanced precipitation in Australia, Andes and eastern Africa, from March to October during the MIS5e (9b,c). Southward to 16°S most proxies are dominated by wetter conditions in Australia and southern Africa.

Some conditions persist along the months, such as the weakening of the ITCZ, that is supported by both modelled precipitation and reconstructions. Brazil and equatorial eastern Africa are also characterized by dryer and wetter conditions, respectively. Little information is available for MIS11c regarding moisture availability, proxies from Africa and South America allow us to infer that during MIS11c conditions were wetter than the current climate. For MIS31 there is scarce information which hampers to derive conclusions from comparison between model outputs in this study. But Justino et al. (2019) argue that the link between the Niño 3.4 and the Australian monsoon is weakened with respect to the CTRL characteristics, and indicates that changes in AUSM during the MIS31 are more closely connected to hemispherical features than to the equatorial climate interaction.

4 Concluding remarks

This study demonstrates that the Austral summer monsoons experienced strong changes during the MIS5e, MIS11c and the MIS31 intervals. This results due to changes in orbital insolation, which further modify the SSTs and global teleconnection patterns. Indeed, changes in the precessional cycle triggered significant cooling across Southern Oceans. In the SAMS region, for example, the MIS5e and MIS11c exhibit a decrease in the transport of moisture from the Amazon to southeastern South America. The contribution of continental dry air mass quantitatively favored the decrease of summer monsoon rainfall, and the intensified reduction of SST during these interglacials, provided a northward displacement of the SASM, as well as of the SACZ.

Changes of monsoonal precipitation have also been delivered in terms of the month with maximum occurrence. Despite weaker precipitation in summer, the MIS5e and MIS11c stages are dominated by enhanced rainfall in the SH winter and early spring, for the SAFM, and winter/autumm for the AUSM. Thus, reduced precipitation is related to colder conditions during the SH summer, in particular over the continents. Correlation analyses indicate that large-scale processes, such as related to ENSO during the interglacials are weaker with respect to CTRL, in exception of increased significant correlation values over the SAMS.

Comparison between palaeoreconstructions and model simulations revealed a good agreement. It is worth noting that the palaeoproxies deliver the main response to a particular forcing, but does not indicate the preferential season of occurrence. Hence, for analysing the modeled precipitation it is necessary to figure out modeled monthly distribution, because as demonstrated in Figure 9, large differences in rainfall between the modelling experiments and CTRL, insofar as monsoonal precipitation is concerned, are found not only for the summer season, but substantial changes have also been found throughout the year.

Climate simulations aiming at reproducing the monsoonal system usefully serve to point out that enhanced Northern Hemisphere warming, can modify the temporal and spatial pattern of Southern Hemisphere precipitation. In a palaeoclimate perspective, this may be understood as analogues of conditions during Dansgaard–Oeschger events by means of the two hemispheres seesaw Stocker and Johnsen (2003). At some extent, global warming that also shows much warmer Boreal climate may also deliver modified SH monsoonal precipitation in line with interglacial conditions, as simulated here. Thus, Earth's future climate can be explored in detail based on climate experiments for past intervals stages. as based on coupled models of intermediate complexity as currently applied.

5 Acknowledgements

The authors want to thank the funding support of CAPES to project Research Group on Climate Interaction (InteraC), a , and CNPq funding 303882/2020. PhD Student Carlos Gurjão and Dr, Flávio Justino designed the study, performed data processing, and plotting, and wrote large portions of the manuscript. Dr. Douglas Lindemann contributed with the model simulations. ERA5 is also acknowledged for providing the reanalysis data set.

References

Abrantes F (2003) A 340,000 year continental climate record from tropical africa–news from opal phytoliths from the equatorial atlantic. Earth and Planetary Science Letters 209(1-2):165–179

Bard E, Hamelin B, Fairbanks RG (1990) U-th ages obtained by mass spectrometry in corals from barbados: sea level during the past 130,000 years. Nature 346(6283):456–458

Bereiter B, Eggleston S, Schmitt J, Nehrbass-Ahles C, Stocker TF, Fischer H, Kipfstuhl S, Chappellaz J (2015) Revision of the epica dome c co2 record from 800 to 600 kyr before present. Geophysical Research Letters 42(2):542–549

Berger A, Loutre MF (1991) Insolation values for the climate of the last 10 million years. Quaternary Science Reviews 10(4):297–317

Bowler JM, Wyrwoll KH, Lu Y (2001) Variations of the northwest australian summer monsoon over the last 300,000 years: the paleohydrological record of the gregory (mulan) lakes system. Quaternary International 83:63–80

Braconnot P, Marzin C, Grégoire L, Mosquet E, Marti O (2008) Monsoon response to changes in Earth's orbital parameters: comparisons between simulations of the Eemian and of the Holocene. Climate of the Past 4(4):281–294

Braconnot P, Harrison S, Kageyama M, Bartlein P, Masson-Delmotte V, Abe-Ouchi A, Otto-Bliesner B, Zhao Y (2012) Evaluation of climate models using palaeoclimate data. Nature Climate Change 2:417–424, DOI 10.1038/NCLIMATE1456

Burrough SL, Thomas DS, Bailey RM (2009) Mega-lake in the kalahari: a late pleistocene record of the palaeolake makgadikgadi system. Quaternary Science Reviews 28(15-16):1392–1411

Cabos W, de la Vara A, Koseki S (2019) Tropical atlantic variability: Observations and modeling. Atmosphere 10(9), URL https://www.mdpi.com/2073-4433/10/9/502

Caley T, Extier T, Collins JA, Schefuß E, Dupont L, Malaizé B, Rossignol L, Souron A, McClymont EL, Jimenez-Espejo FJ, et al. (2018) A two-million-year-long hydroclimatic context for hominin evolution in southeastern africa. Nature 560(7716):76–79

Carolin SA, Cobb KM, Lynch-Stieglitz J, Moerman JW, Partin JW, Lejau S, Malang J, Clark B, Tuen AA, Adkins JF (2016) Northern borneo stalagmite records reveal west pacific hydroclimate across mis 5 and 6. Earth and Planetary Science Letters 439:182–193

Cheng H, Sinha A, Cruz FW, Wang X, Edwards RL, d'Horta FM, Ribas CC, Vuille M, Stott LD, Auler AS (2013) Climate change patterns in amazonia and biodiversity. Nature communications 4(1):1–6

Coletti A, DeConto R, Brigham-Grette J, Melles M (2015) A gcm comparison of pleistocene super-interglacial periods in relation to lake el'gygytgyn, ne arctic russia. Climate of the Past 11(7)

Collini EA, Berbery EH, Barros VR, Pyle ME (2008) How does soil moisture influence the early stages of the south american monsoon? Journal of Climate 21(2):195–213, DOI https://doi.org/10.1175/2007JCLI1846.1

Collins JA, Schefuß E, Govin A, Mulitza S, Tiedemann R (2014) Insolation and glacial–interglacial control on southwestern african hydroclimate over the past 140 000 years. Earth and Planetary Science Letters 398:1–10

Contreras S, Lange CB, Pantoja S, Lavik G, Rincón-Martínez D, Kuypers MM (2010) A rainy northern atacama desert during the last interglacial. Geophysical Research Letters 37(23)

Crundwell M, Scott G, Naish T, Carter L (2008) Glacial–interglacial ocean climate variability from planktonic foraminifera during the mid-pleistocene transition in the temperate southwest pacific, odp site 1123. Palaeogeography, Palaeoclimatology, Palaeoecology 260(1-2):202–229

Dang H, Jian Z, Kissel C, Bassinot F (2015) Precessional changes in the western equatorial p acific hydroclimate: A 240 kyr marine record from the h almahera s ea, e ast i ndonesia. Geochemistry, Geophysics, Geosystems 16(1):148–164

Daniau AL, Goñi MFS, Martinez P, Urrego DH, Bout-Roumazeilles V, Desprat S, Marlon JR (2013) Orbital-scale climate forcing of grassland burning in southern africa. Proceedings of the National Academy of Sciences 110(13):5069–5073

Deng K, Yang S, Ting M, Tan Y, He S (2018) Global monsoon precipitation: Trends, leading modes, and associated drought and heat wave in the northern hemisphere. Journal of Climate 31(17):6947–6966, DOI https://doi.org/10.1175/JCLI-D-17-0569.1

Diaz M, Boos WR (2021) The Influence of Surface Heat Fluxes on the Growth of Idealized Monsoon Depressions. Journal of the Atmospheric Sciences 78(6):2013 – 2027, DOI 10.1175/JAS-D-20-0359.1, URL https://journals.ametsoc.org/view/journals/atsc/78/6/JAS-D-20-0359.1.xml

Dickson AJ, Leng MJ, Maslin MA, Röhl U (2010) Oceanic, atmospheric and ice-sheet forcing of south east atlantic ocean productivity and south african monsoon intensity during mis-12 to 10. Quaternary Science Reviews 29(27-28):3936–3947

Dupont LM, Kuhlmann H (2017) Glacial-interglacial vegetation change in the zambezi catchment. Quaternary Science Reviews 155:127–135

Dyez KA, Ravelo AC (2014) Dynamical changes in the tropical pacific warm pool and zonal sst gradient during the pleistocene. Geophysical Research Letters 41(21):7626–7633

Ávila Díaz Justino F, Wilson A, Bromwich D, Amorim M (2016) Recent precipitation trends, flash floods and landslides in southern brazil. Environmental Research Letters 11:1–13, DOI 10.1088/1748-9326/11/11/114029

D'Agostino R, Brown JR, Moise AF, Nguyen H, Dias PLS, Jungclaus JH (2020) Contrasting southern hemisphere monsoon response: Mid-holocene orbital forcing versus future greenhouse gas–induced global warming. Journal of Climate 33:9595–9613, DOI https://doi.org/10.1175/JCLI-D-19-0672.1

Flato G, Marotzke J, Abiodun B, Braconnot P, Chou SC, Collins W, Cox P, Driouech F, Emori S, Eyring V, et al. (2014) Evaluation of climate models. In: Climate change 2013: the physical science basis. Contribution of Working Group I to the Fifth Assessment Report of the Intergovernmental Panel on Climate Change, Cambridge University Press, pp 741–866

Frédoux A (1994) Pollen analysis of a deep-sea core in the gulf of guinea: vegetation and climatic changes during the last 225,000 years bp. Palaeogeography, Palaeoclimatology, Palaeoecology 109(2-4):317–330

Fritz SC, Baker PA, Lowenstein TK, Seltzer GO, Rigsby CA, Dwyer GS, Tapia PM, Arnold KK, Ku TL, Luo S (2004) Hydrologic variation during the last 170,000 years in the southern hemisphere tropics of south america. Quaternary Research 61(1):95–104 de Garidel-Thoron T, Rosenthal Y, Bassinot F, Beaufort L (2005) Stable sea surface temperatures in the western pacific warm pool over the past 1.75 million years. Nature 433(7023):294–298

Geen R, Bordoni S, Battisti DS, Hui K (2020) Monsoons, ITCZs, and the concept of the global monsoon. Reviews of Geophysics 58(4):e2020RG000700

Gingele F, Müller P, Schneider R (1998) Orbital forcing of freshwater input in the zaire fan area—clay mineral evidence from the last 200 kyr. Palaeogeography, Palaeoclimatology, Palaeoecology 138(1-4):17–26

Gosling WD, Bush MB, Hanselman JA, Chepstow-Lusty A (2008) Glacial-interglacial changes in moisture balance and the impact on vegetation in the southern hemisphere tropical andes (bolivia/peru). Palaeogeography, Palaeoclimatology, Palaeoecology 259(1):35–50

Govin A, Chiessi CM, Zabel M, Sawakuchi A, Heslop D, Hörner T, Zhang Y, Mulitza S (2014) Terrigenous input off northern south america driven by changes in amazonian climate and the north brazil current retroflection during the last 250 ka. Climate of the Past 10(2):843–862

Ha KJ, Kim BH, Chung ES, Chan JCL, Chang CP (2020) Major factors of global and regional monsoon rainfall changes: natural versus anthropogenic forcing. Environmental Research Letters 15(3):034055, DOI 10.1088/1748-9326/ab7767, URL https://doi.org/10.1088/1748-9326/ab7767

Hayward BW, Sabaa AT, Kolodziej A, Crundwell MP, Steph S, Scott GH, Neil HL, Bostock HC, Carter L, Grenfell HR (2012) Planktic foraminifera-based sea-surface temperature record in the tasman sea and history of the subtropical front around new zealand, over the last one million years. Marine Micropaleontology 82:13–27

Held IM, Soden BJ (2006) Robust responses of the hydrological cycle to global warming. Journal of climate 19(21):5686–5699, DOI https://doi.org/10.1175/JCLI3990.1

Herbert T, Schuffert J, Andreasen D, Heusser L, Lyle M, Mix A, Ravelo A, Stott L, Herguera J (2001) Collapse of the california current during glacial maxima linked to climate change on land. Science 293(5527):71–76

Herbert TD, Peterson LC, Lawrence KT, Liu Z (2010a) Tropical ocean temperatures over the past 3.5 million years. science 328(5985):1530–1534

Herbert TD, Peterson LC, Lawrence KT, Liu Z (2010b) Tropical ocean temperatures over the past 3.5 million years. science 328(5985):1530–1534

Herbert TD, Peterson LC, Lawrence KT, Liu Z (2010c) Tropical ocean temperatures over the past 3.5 million years. science 328(5985):1530–1534

Hersbach H (2016) The era5 atmospheric reanalysis. AGUFM 2016:NG33D–01

Ho SL, Mollenhauer G, Lamy F, Martínez-Garcia A, Mohtadi M, Gersonde R, Hebbeln D, Nunez-Ricardo S, Rosell-Melé A, Tiedemann R (2012) Sea surface temperature variability in the pacific sector of the southern ocean over the past 700 kyr. Paleoceanography 27(4)

Horikawa K, Murayama M, Minagawa M, Kato Y, Sagawa T (2010) Latitudinal and downcore (0–750 ka) changes in nalkane chain lengths in the eastern equatorial pacific. Quaternary Research 73(3):573–582

Hou A, Bahr A, Schmidt S, Strebl C, Albuquerque AL, Chiessi CM, Friedrich O (2020) Forcing of western tropical south atlantic sea surface temperature across three glacial-interglacial cycles. Global and Planetary Change 188:103150

Ivory SJ, Blome MW, King JW, McGlue MM, Cole JE, Cohen AS (2016) Environmental change explains cichlid adaptive radiation at lake malawi over the past 1.2 million years. Proceedings of the National Academy of Sciences 113(42):11895–11900

Jorgetti T, Silva Dias P, Freitas E (2014) The relationship between south atlantic sst and sacz intensity and positioning. Clim Dyn 42:3077–3086, DOI 10.1007/s00382-013-1998-z

Justino F, Lindemann D, Kucharski F, Wilson A, Bromwich D, Stordal F (2017) Oceanic response to changes in the WAIS and astronomical forcing during the MIS31 superinterglacial. Climate of the Past 13(9):1081–1095

Justino F, Kucharski F, Lindemann D, Wilson A, Stordal F (2019) A modified seasonal cycle during MIS31 super-interglacial favors stronger interannual ENSO and monsoon variability. Climate of the Past 15(2):735–749

Justino F, Gurjão C, Lindemann D (2021) Climate response to drastically modified PDO, PNA and NAM in the superinterglacial MIS 31. Boreas DOI https://doi.org/10.1111/bor.12556

Van der Kaars W, Dam M (1995) A 135,000-year record of vegetational and climatic change from the bandung area, west-java, indonesia. Palaeogeography, Palaeoclimatology, Palaeoecology 117(1-2):55–72

Kawamura H, Holbourn A, Kuhnt W (2006) Climate variability and land–ocean interactions in the indo pacific warm pool: a 460-ka palynological and organic geochemical record from the timor sea.

Marine Micropaleontology 59(1):1–14

Kemp C, Tibby J, Arnold L, Barr C, Gadd P, Marshall J, McGregor G, Jacobsen G (2020) Climates of the last three interglacials in subtropical eastern australia inferred from wetland sediment geochemistry. Palaeogeography, Palaeoclimatology, Palaeoecology 538:109463

Kucharski F, Molteni F, Bracco A (2006) Decadal interactions between the western tropical pacific and the north atlantic oscillation. Climate dynamics 26(1):79–91

Kucharski F, Ikram F, Molteni F, Farneti R, Kang IS, No HH, King MP, Giuliani G, Mogensen K (2016) Atlantic forcing of pacific decadal variability. Climate dynamics 46(7-8):2337–2351

Kundzewicz ZW, Kanae S, Seneviratne SI, Handmer J, Nicholls N, Peduzzi P, Mechler R, Bouwer LM, Arnell N, Mach K, Muir-Wood R, Brakenridge GR, Kron W, Benito G, Honda Y, Takahashi K, Sherstyukov B (2014) Flood risk and climate change: global and regional perspectives. Hydrological Sciences Journal 59(1):1–28, DOI 10.1080/02626667.2013.857411, URL https://doi.org/10.1080/02626667.2013.857411, https://doi.org/10.1080/02626667.2013.857411

Lawrence KT, Herbert TD, Brown CM, Raymo ME, Haywood AM (2009) High-amplitude variations in north atlantic sea surface temperature during the early pliocene warm period. Paleoceanography 24(2)

Lea DW, Pak DK, Spero HJ (2000) Climate impact of late quaternary equatorial pacific sea surface temperature variations. science 289(5485):1719–1724

Lea DW, Pak DK, Belanger CL, Spero HJ, Hall MA, Shackleton NJ (2006) Paleoclimate history of galápagos surface waters over the last 135,000 yr. Quaternary Science Reviews 25(11-12):1152–1167

Li L, Li Q, Tian J, Wang P, Wang H, Liu Z (2011) A 4-ma record of thermal evolution in the tropical western pacific and its implications on climate change. Earth and Planetary Science Letters 309(1-2):10–20

Li X, Ting M (2017) Understanding the Asian summer monsoon response to greenhouse warming: the relative roles of direct radiative forcing and sea surface temperature change. Climate Dynamics 49(7-8):2863–2880, DOI 10.1007/s00382-016-3470-3

Lisiecki LE, Raymo ME (2005) A pliocene-pleistocene stack of 57 globally distributed benthic δ18o records. Paleoceanography 20(1)

Liu Z, Altabet MA, Herbert TD (2005) Glacial-interglacial modulation of eastern tropical north pacific denitrification over the last 1.8-myr. Geophysical Research Letters 32(23)

Liu Z, Zhu J, Rosenthal Y, Zhang X, Otto-Bliesner B, Timmermann A, Smith R, Lohmann G, Zheng W, Timm O (2014) The holocene temperature conundrum. Proceedings of the National Academy of Sciences 111, DOI 10.1073/pnas.1407229111

Lo L, Chang SP, Wei KY, Lee SY, Ou TH, Chen YC, Chuang CK, Mii HS, Burr GS, Chen MT, et al. (2017) Nonlinear climatic sensitivity to greenhouse gases over past 4 glacial/interglacial cycles. Scientific reports 7(1):1–7

Lückge A, Mohtadi M, Rühlemann C, Scheeder G, Vink A, Reinhardt L, Wiedicke M (2009) Monsoon versus ocean circulation controls on paleoenvironmental conditions off southern sumatra during the past 300,000 years. Paleoceanography 24(1)

Lüthi D, Le Floch M, Bereiter B, Blunier T, Barnola JM, Siegenthaler U, Raynaud D, Jouzel J, Fischer H, Kawamura K, et al. (2008) High-resolution carbon dioxide concentration record 650,000–800,000 years before present. Nature 453(7193):379

Madec G (2008) Nemo ocean engine. note du pole de modélisation, institut pierre-simon laplace (ipsl). France 27:1288–1619

Madec G (2012) Nemo ocean engine. note du pole de modélisation de l'institut pierre-simon laplace, france, no. 27. issn no. 1288–1619

Madec G, Delecluse P, Imbard M, Lévy C (1998) Opa 8.1 ocean general circulation model reference manual. Note du Pôle de modélisation 11:91p

Magee JW, Miller GH, Spooner NA, Questiaux D (2004) Continuous 150 ky monsoon record from lake eyre, australia: insolation-forcing implications and unexpected holocene failure. Geology 32(10):885–888

Marengo JA, Liebmann B, Grimm AM, Misra V, Silva Dias PL, Cavalcanti IFA, Carvalho LMV, Berbery EH, Ambrizzi T, Vera CS, Saulo AC, Nogues-Paegle J, Zipser E, Seth A, Alves LM (2012) Recent developments on the south american monsoon system. International Journal of Climatology 32(1):1–21, DOI https://doi.org/10.1002/joc.2254, URL https://rmets.onlinelibrary.wiley.com/doi/abs/10.1002/joc.2254, https://rmets.onlinelibrary.wiley.com/doi/pdf/10.1002/joc.2254

Martínez-Garcia A, Rosell-Melé A, McClymont EL, Gersonde R, Haug GH (2010) Subpolar link to the emergence of the modern equatorial pacific cold tongue. Science 328(5985):1550–1553

McClymont EL, Rosell-Melé A (2005) Links between the onset of modern walker circulation and the mid-pleistocene climate transition. Geology 33(5):389–392

McClymont EL, Rosell-Melé A, Giraudeau J, Pierre C, Lloyd JM (2005) Alkenone and coccolith records of the mid-pleistocene in the south-east atlantic: Implications for the u37k index and south african climate. Quaternary Science Reviews 24(14-15):1559–1572

McPhaden MJ, Zebiak SE, Glantz MH (2006) Enso as an integrating concept in earth science. Science 314(5806):1740–1745, DOI 10.1126/science.1132588

Medina-Elizalde M, Lea DW (2005) The mid-pleistocene transition in the tropical pacific. Science 310(5750):1009–1012

Medina-Elizalde M, Lea DW, Fantle MS (2008) Implications of seawater mg/ca variability for plio-pleistocene tropical climate reconstruction. Earth and Planetary Science Letters 269(3-4):585–595

Melles M, Brigham-Grette J, Minyuk PS, Nowaczyk NR, Wennrich V, DeConto RM, Anderson PM, Andreev AA, Coletti A, Cook TL, et al. (2012) 2.8 million years of arctic climate change from lake el'gygytgyn, ne russia. science 337(6092):315–320

Members CLIP (2006) Last interglacial arctic warmth confirms polar amplification of climate change. Quaternary Science Reviews 25(13-14):1383–1400

Miller GH, Fogel ML, Magee JW, Gagan MK (2016) Disentangling the impacts of climate and human colonization on the flora and fauna of the australian arid zone over the past 100 ka using stable isotopes in avian eggshell. Quaternary Science Reviews 151:27–57

Moernaut J, Verschuren D, Charlet F, Kristen I, Fagot M, De Batist M (2010) The seismic-stratigraphic record of lake-level fluctuations in lake challa: Hydrological stability and change in equatorial east africa over the last 140 kyr. Earth and Planetary Science Letters 290(1-2):214–223

Molteni F (2003) Atmospheric simulations using a GCM with simplified physical parametrizations. I: Model climatology and variability in multi-decadal experiments. Climate Dynamics pp 175–191, DOI 10.1007/s00382-002-0268-2

Montoya M, von Storch H, Crowley TJ (2000) Climate simulation for 125 kyr bp with a coupled ocean–atmosphere general circulation model. Journal of Climate 13(6):1057–1072

Moss PT, Kershaw AP (2007) A late quaternary marine palynological record (oxygen isotope stages 1 to 7) for the humid tropics of northeastern australia based on odp site 820. Palaeogeography, Palaeoclimatology, Palaeoecology 251(1):4–22

Naafs BDA, Hefter J, Gruetzner J, Stein R (2013) Warming of surface waters in the mid-latitude north atlantic during heinrich events. Paleoceanography 28(1):153–163

Neelin JD, Latif M, Jin F (1994) Dynamics of coupled ocean-atmosphere models: The tropical problem. Annual Review of Fluid Mechanics 26(1):617–659, DOI 10.1146/annurev.fl.26.010194.003153

Nogués-Paegle J, Mechoso CR, Fu R, Berbery EH, Chao WC, Chen TC, Cook K, Diaz AF, Enfield D, Ferreira R, et al. (2002) Progress in pan american clivar research: understanding the south american monsoon. Meteorologica 27(12):1–30

Oliveira D, Sánchez Goñi MF, Naughton F, Polanco-Martínez J, Jimenez-Espejo FJ, Grimalt JO, Martrat B, Voelker AH, Trigo R, Hodell D, Abrantes F, Desprat S (2017) Unexpected weak seasonal climate in the western mediterranean region during mis 31, a high-insolation forced interglacial. Quaternary Science Reviews 161:1–17, DOI https://doi.org/10.1016/j.quascirev.2017.02.013, URL https://www.sciencedirect.com/science/article/pii/S0277379116306515

Oppo D, McManus J, Cullen J (1998) Abrupt climate events 500,000 to 340,000 years ago: Evidence from subpolar north atlantic sediments. Science 279(5355):1335–1338

Owen RB, Muiruri VM, Lowenstein TK, Renaut RW, Rabideaux N, Luo S, Deino AL, Sier MJ, Dupont-Nivet G, McNulty EP, et al. (2018) Progressive aridification in east africa over the last half million years and implications for human evolution. Proceedings of the National Academy of Sciences 115(44):11174–11179

Partridge T, Demenocal P, Lorentz S, Paiker M, Vogel J (1997) Orbital forcing of climate over south africa: a 200,000-year rainfall record from the pretoria saltpan. Quaternary Science Reviews 16(10):1125–1133

Pezzi L, Quadro M, Lorenzzetti J, Miller A, Rosa E, Lima L, Sutil U (2022) The effect of oceanic south atlantic convergence zone episodes on regional sst anomalies: the roles of heat fluxes and upper-ocean dynamics. Climate Dynamics pp 1–25, DOI 10.1007/s00382-022-06195-3

Placzek C, Quade J, Patchett P (2013) A 130 ka reconstruction of rainfall on the bolivian altiplano. Earth and Planetary Science Letters 363:97–108

Raymo M, Grant B, Horowitz M, Rau G (1996) Mid-pliocene warmth: stronger greenhouse and stronger conveyor. Marine Micropaleontology 27(1-4):313–326

Rincón-Martínez D, Lamy F, Contreras S, Leduc G, Bard E, Saukel C, Blanz T, Mackensen A, Tiedemann R (2010) More humid interglacials in ecuador during the past 500 kyr linked to latitudinal shifts of the equatorial front and the intertropical convergence zone in the eastern tropical pacific. Paleoceanography 25(2)

Ritter B, Wennrich V, Medialdea A, Brill D, King G, Schneiderwind S, Niemann K, Fernández-Galego E, Diederich J, Rolf C, et al. (2019) Climatic fluctuations in the hyperarid core of the atacama desert during the past 215 ka. Scientific reports 9(1):1–13

Rousseau DD, Puisségur JJ, Lécolle F (1992) West-european terrestrial molluscs assemblages of isotopic stage 11 (middle pleistocene): climatic implications. Palaeogeography, Palaeoclimatology, Palaeoecology 92(1-2):15–29

Ruddiman W, Shackleton N, McIntyre A (1986) North atlantic sea-surface temperatures for the last 1.1 million years. Geological Society, London, Special Publications 21(1):155–173

Ruddiman WF, Raymo M, Martinson D, Clement B, Backman J (1989) Pleistocene evolution: Northern hemisphere ice sheets and north atlantic ocean. Paleoceanography 4(4):353–412

Russon T, Elliot M, Sadekov A, Cabioch G, Corrège T, De Deckker P (2011) The mid-pleistocene transition in the subtropical southwest pacific. Paleoceanography 26(1)

Schaefer G, Rodger JS, Hayward BW, Kennett JP, Sabaa AT, Scott GH (2005) Planktic foraminiferal and sea surface temperature record during the last 1 myr across the subtropical front, southwest pacific. Marine Micropaleontology 54(3-4):191–212

Siccha M, Biton E, Gildor H (2015) Red sea circulation during marine isotope stage 5e. Paleoceanography 30(4):384–401

Simon MH, Ziegler M, Bosmans J, Barker S, Reason CJ, Hall IR (2015) Eastern south african hydroclimate over the past 270,000 years. Scientific Reports 5(1):1–10

Stocker TF, Johnsen SJ (2003) A minimum thermodynamic model for the bipolar seesaw. Paleoceanography 18(4):1087, DOI 10.1029/2003PA000920

Stuut JBW, Prins MA, Schneider RR, Weltje GJ, Jansen JF, Postma G (2002) A 300-kyr record of aridity and wind strength in southwestern africa: inferences from grain-size distributions of sediments on walvis ridge, se atlantic. Marine Geology 180(1-4):221–233

Stuut JBW, Temmesfeld F, De Deckker P (2014) A 550 ka record of aeolian activity near north west cape, australia: inferences from grain-size distributions and bulk chemistry of se indian ocean deep-sea sediments. Quaternary Science Reviews 83:83–94

Trauth MH, Deino A, Strecker MR (2001) Response of the east african climate to orbital forcing during the last interglacial (130–117 ka) and the early last glacial (117–60 ka). Geology 29(6):499–502

Trenberth K, Stepaniak D, Caron J (2000) The global monsoon as seen through the divergent atmospheric circulation. J of Climate 13(22):3969–3993, DOI 10.1175/1520-0442(2000)013¡3969:TGMAST¿2.0.CO;2

Uliana E, Lange CB, Wefer G (2002) Evidence for congo river freshwater load in late quaternary sediments of odp site 1077 (5 s, 10 e). Palaeogeography, Palaeoclimatology, Palaeoecology 187(1-2):137–150

Valcke S (2013) The oasis3 coupler: a european climate modelling community software. Geoscientific Model Development 6(2):373–388

Weldeab S, Lea DW, Schneider RR, Andersen N (2007) 155,000 years of west african monsoon and ocean thermal evolution. science 316(5829):1303–1307

Wild M (2020) The global energy balance as represented in cmip6 climate models. Climate Dynamics 55:553–577, DOI https://doi.org/10.1007/s00382-020-05282-7

Windler G, Tierney JE, DiNezio PN, Gibson K, Thunell R (2019) Shelf exposure influence on indo-pacific warm pool climate for the last 450,000 years. Earth and Planetary Science Letters 516:66–76

Yim SY, Wang B, Liu J, Wu Z (2014) A comparison of regional monsoon variability using monsoon indices. Climate dynamics 43(5-6):1423–1437

Yin Q, Berger A (2012) Individual contribution of insolation and CO2 to the interglacial climates of the past 800,000 years. Climate Dynamics 38:709–724, DOI 10.1007/s00382-011-1013-5

Yin Q, Singh UK, Berger A, Guo ZT, Crucifix M (2014) Relative impact of insolation and the Indo-Pacific warm pool surface temperature on the East Asia summer monsoon during the MIS-13 interglacial. Climate of the Past 10(5):1645–1657, DOI 10.5194/cp-10-1645-2014, URL https://cp.copernicus.org/articles/10/1645/2014/

Zeng J, Zhang Q (2020) The trends in land surface heat fluxes over global monsoon domains and their responses to monsoon and precipitation. Scientific reports 10(1):1–15

Zhao X, Cheng H, Sinha A, Zhang H, Baker JL, Chen S, Kong X, Wang Y, Edwards RL, Ning Y, et al. (2019) A high-resolution speleothem record of marine isotope stage 11 as a natural analog to holocene asian summer monsoon variations. Geophysical Research Letters 46(16):9949–9957

Table 1 Orbital configurations and greenhouse gases concentrations utilized in the CTRL, MIS5e, MIS11c and MIS31 experiments.

Experiment	Date	CO_2(ppmv)	CH_4(ppbv)	N_2O(ppbv)	Ecc.	Obl.	Prec.
CTRL	Present	380	801	289	0.01671	23.438	101.37
MIS5e	127 ka BP	287	724	262	0.03938	24.040	272.92
MIS11c	409 ka BP	285	713	285	0.01932	23.781	265.34
MIS31	1.072 ka BP	325	800	288	0.05597	23.898	289.79

Table 2 Correlation coefficients between the regional monsoon precipitation in the rectangular domains and respective vorticity indices. Bold values indicate statistical significance at the 95% level.

	Monsoon Domain	Monsoon (index)	ERA5 CC	CTRL CC	MIS5e CC	MIS11c CC	MIS31 CC
SAFSM	(0-20°S,10°E-50°E)	U_{850}(5°S-15°S, 20°E-50°E) - U_{850}(20°S-30°S, 30°E-55°E)	**0,52**	**0,74**	**0,76**	**0,78**	**0,77**
AUSSM	(0-20°S,105°E-160°E)	U_{850}(0-15°S, 90°E-130°E) - U_{850}(20°S-30°S, 100°E-140°E)	**0,93**	**0,86**	**0,72**	**0,74**	**0,73**
SASM	(5°S-25°S,70°W-40°W)	U_{850}(5°S-20°S, 90°E-130°E) - U_{850}(20°S-30°S, 100°E-140°E)	**0,80**	**0,37**	**0,50**	**0,65**	**0,31**

Table 3 Correlation coefficients between Niño 3.4, TAV indices and the regional monsoon precipitation. Bold values indicate statistical significance at the 95% level.

	ERA5		CTRL		MIS5e		MIS11c		MIS31	
Austral Summer (DJFM)										
Index	Niño 3.4	TAV	Niño 3.4	TAV	Niño 3.4	TAV	Niño 3.4	TAV	Niño 3.4	TAV
Monsoon Domain										
SAFSM	**-0.40**	-0.25	**-0.36**	**0.26**	**-0.33**	0.14	**-0.27**	0.1	-0.14	0.13
AUSSM	**-0.70**	0.26	**-0.56**	0.16	-0.05	0.01	-0.04	-0.14	**-0.30**	0.04
SASM	**-0.30**	**0.30**	**-0.20**	0.18	**-0.29**	**-0.33**	**-0.23**	-0.11	-0.03	-0.15

Table 4 Maximum values of SST records and modeling results for each interglacial. R represents values of reconstruction. Δ_{SST}(°C) shows differences between ICTP-CGCM results and R.

Site	Coordinates	MIS5e R Δ_{SST}	MIS11c R Δ_{SST}	MIS31 R Δ_{SST}	References
Lake E	67°N-172°E	14.5 [-0.32]	12.2 [1.3]	14.3 [-1.8]	Melles et al. (2012)
ODP 982	57°N-15°W	16.2 [0.71]	15.0 [1.49]	13.8 [-3.0]	Lawrence et al. (2009)
DSDP 552s	56°N-23°W	15.1 [2.31]	16.4 [0.05]		Ruddiman et al. (1986)
DSDP607	41°N-31°W	29.1 [1.4]		17.5 [-0.6]	Raymo et al. (1996)
306-U1313	41°N-32°W			18.0 [-1.1]	Naafs et al. (2013)
ODP 1020	41°N-126°W	14.1 [6.41]	14.0 [6.37]		Herbert et al. (2001)
DSDP 607s	56°N-32°W	25.1 [-0.53]	26.8 [-3.42]		Ruddiman et al. (1989)
ODP 1012	32°N-118°W	19.5 [-0.05]	19.1 [5.9]		Liu et al. (2005)
ODP 1146	19°N-116°E	27.3 [3.94]	26.8 [3.73]	26.0 [-1.0]	Herbert et al. (2010a)
ODP 722	16°N-60°E	27.7 [3.51]	27.5 [3.36]	27.0 [1.0]	Herbert et al. (2010b)
ODP 1143	9°N-113°E	28.8 [3.14]	28.3 [3.0]	28.3 [-0.8]	Li et al. (2011)
ODP 871	5°N-172°E			29.3 [-0.4]	Dyez and Ravelo (2014)
HY04	4°N-95°W	27.2 [1.34]	26.3 [2.19]		Horikawa et al. (2010)
MD97-2140	2°N-141°E	29.5 [0.14]	29.5 [0.58]		de Garidel-Thoron et al. (2005)
ODP 806B	0.3°N-159°E	29.6 [1.03]	30.2 [-0.08]		Medina-Elizalde and Lea (2005)
ODP 847	0-95°W			25.6 [-0.6]	Medina-Elizalde et al. (2008)
ODP 849	0-110°W			25.8 [-0.8]	McClymont and Rosell-Melé (2005)
ODP 846	3°S-90°W	25.1 [0.69]	24.0 [2.49]	24.3 [0.5]	Herbert et al. (2010c)
MD-06-301	23°S-166°E			25.0 [-1.1]	Russon et al. (2011)
ODP 1087	31°S-15°E			18.0 [-0.3]	McClymont et al. (2005)
ODP 1123	41°S-171°W	17.7 [-0.61]	19.3 [-3.25]	16.0 [0.8]	Crundwell et al. (2008)
ODP 1090	43°S-9°E	17.1 [-2.16]	13.9 [0.14]	11.5 [-1.7]	Martínez-Garcia et al. (2010)
MD06-2986	43°S-168°E	18.0 [-3.12]	18.1 [-2.51]		Hayward et al. (2012)
DSDP594	45°S-175°E	18.3 [-4.9]	17.5 [-5.85]		Schaefer et al. (2005)
PS75/034-2	54°S-80°W	10.3 [-0.03]	8.8 [2.19]		Ho et al. (2012)

Table 5 Hydroclimate reconstruction and modeled values for MIS5e, MIS11c and MIS31. Values indicate wet or dry conditions in reconstructions.

Site	Coordinates	MIS5e	MIS11c	MIS31	References
GeoB4411-2	5°N - 44°W	Wet			Govin et al. (2014)
Gunung Mulu	4°N - 114°E	Dry			Carolin et al. (2016)
KS 84067	4°N - 4°W	Wet			Frédoux (1994)
MD03-2707	2°N - 9°E	Dry			Weldeab et al. (2007)
TR163-19	2°N - 90°W	Dry			Lea et al. (2000)
TR163-22	0.5°N - 92°W	Dry			Lea et al. (2006)
Lake Magadi	0.1°S - 36°E	Wet			Owen et al. (2018)
MD01-3340	0.3°S - 128°E	Dry			Dang et al. (2015)
ODP 1239	0.4°S - 82°W	Wet	Wet		Rincón-Martínez et al. (2010)
Lake Naivasha	0.5°S - 36°E	Wet			Trauth et al. (2001)
M16772	1°S - 11°W	Dry			Abrantes (2003)
Lake Challa	3°S - 37°E	Dry			Moernaut et al. (2010)
ODP 1077	5°S - 10°E	Dry			Uliana et al. (2002)
Cueva del Diamante	5°S - 77°W	Wet			Cheng et al. (2013)
SO139-74KL	6°S - 103°E	Dry			Lückge et al. (2009)
MD98-2152	6°S - 104°E	Wet			Windler et al. (2019)
GeoB1401-4	6°S - 9°E	Wet			Gingele et al. (1998)
GeoB1008-3	6°S - 10°E	Wet			Govin et al. (2014)
DPDR-I, DPDR-II	7°S - 108°E	Wet			Van der Kaars and Dam (1995)
MD05-2925	9°S - 151°E	Wet			Lo et al. (2017)
ODP 1229	10°S - 77°W	Wet			Contreras et al. (2010)
GLAD7-MAL05-1	11°S - 34°E	Dry	Wet		Ivory et al. (2016)
MD01-2378	13°S - 121°E	Wet			Kawamura et al. (2006)
Altiplano	16°S - 68°W	Wet			Placzek et al. (2013)
Lake Titicaca, LT01-2B	16°S - 70°W	Dry			Gosling et al. (2008)
Lynch's Crater	17°S - 145°E	Wet			Moss and Kershaw (2007)
MD96-2094	19°S - 9°E	Dry			Stuut et al. (2002)
Gregory(Mulan)	20°S - 127°E	Wet			Bowler et al. (2001)
Salar de Uyuni	20°S - 67°W	Dry			Fritz et al. (2004)
Kalahari - Makgadikgadi	20°S - 25°E	Wet			Burrough et al. (2009)
M125-55-7/8	20°S - 38°W	Dry			Hou et al. (2020)
Coastal Cordillera	21°S - 70°W	Dry			Ritter et al. (2019)
GeoB3911-1	21°S - 36°E	Dry			Dupont and Kuhlmann (2017)
MD00-2361	22°S - 113°E	Dry			Stuut et al. (2014)
MD08-3167	23°S - 12°E	Wet			Collins et al. (2014)
Pretoria Saltpan	25°S - 28°E	Wet			Partridge et al. (1997)
MD96-2098	25°S - 13°E	Dry			Daniau et al. (2013)
MD96-2048	26°S - 34°E	Dry			Caley et al. (2018)
Frern Gully Lagoon	27°S - 153°E	Wet			Kemp et al. (2020)
Lake Eyre	28°S - 137°E	Wet			Magee et al. (2004)
ODP1085	29°S - 13°E		Wet		Dickson et al. (2010)
KT-LE	29°S - 137°E	Wet			Miller et al. (2016)
Frome	30°S - 139°E	Wet			Miller et al. (2016)
CD154-10-06P	31°S - 9°E	Dry			Simon et al. (2015)
PA	32°S - 137°E	Dry			Miller et al. (2016)
Darling	33°S - 144°E	Wet			Miller et al. (2016)

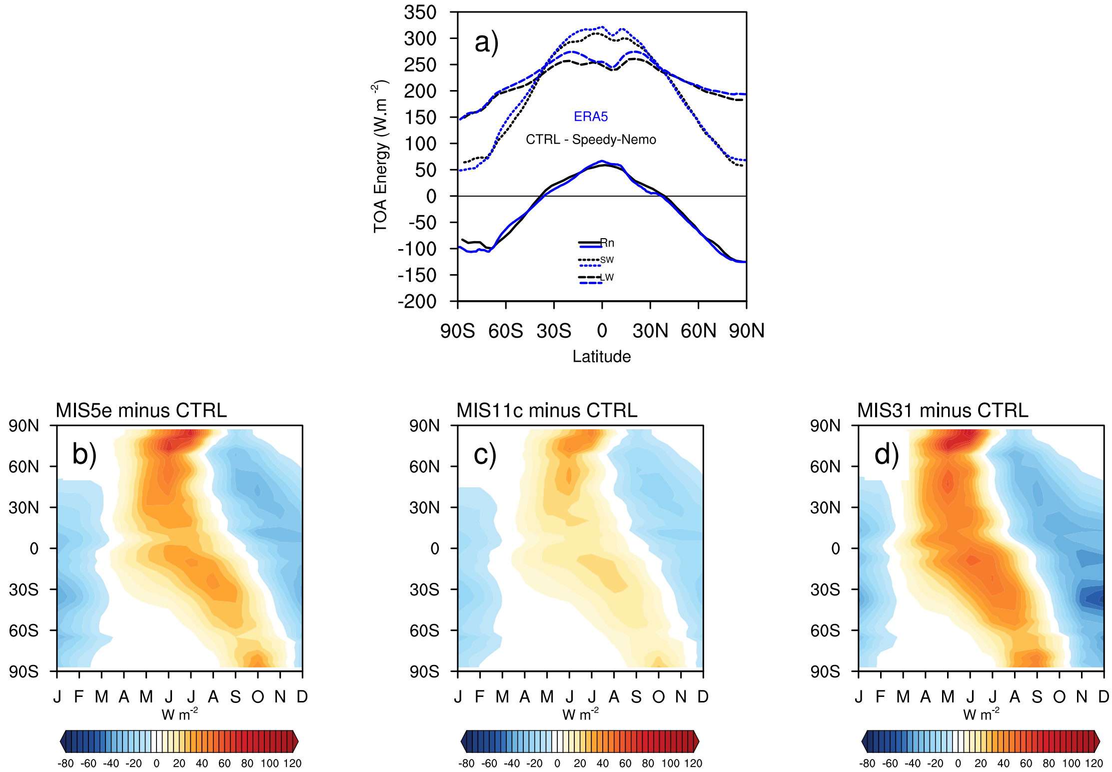

Fig. 1 Zonal mean energy budget components (Wm^{-2}) in the top-of-atmosphere (TOA)(a). (b) shows differences of shortwave radiation at the top of the atmosphere ($W.m^{-2}$) between MIS-5E minus CTRL, MIS-11C minus CTRL (c) and MIS-31 minus CTRL (d). Values in (a) are based on ERA5 reanalysis and the ICTP-CGCM coupled model.

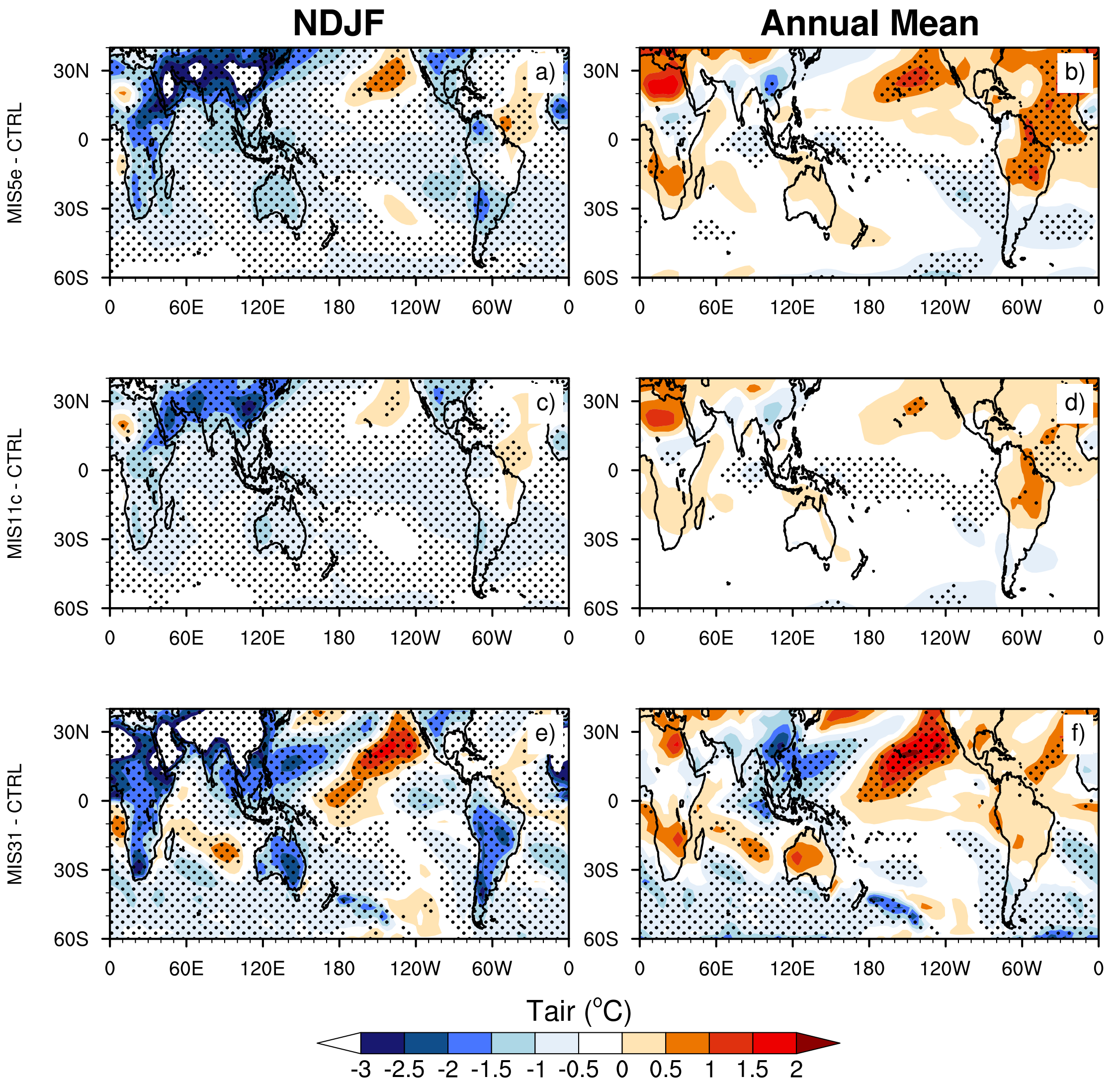

Fig. 2 NDJF mean surface temperature differences (°C) between MIS5e and CTRL (a), MIS11c and CTRL(c), and MIS31 and CTRL (e). (b-d-f) is the same as (a-c-e) but for mean annual differences. Dotted regions are statistically significant at the 95% confidence level.

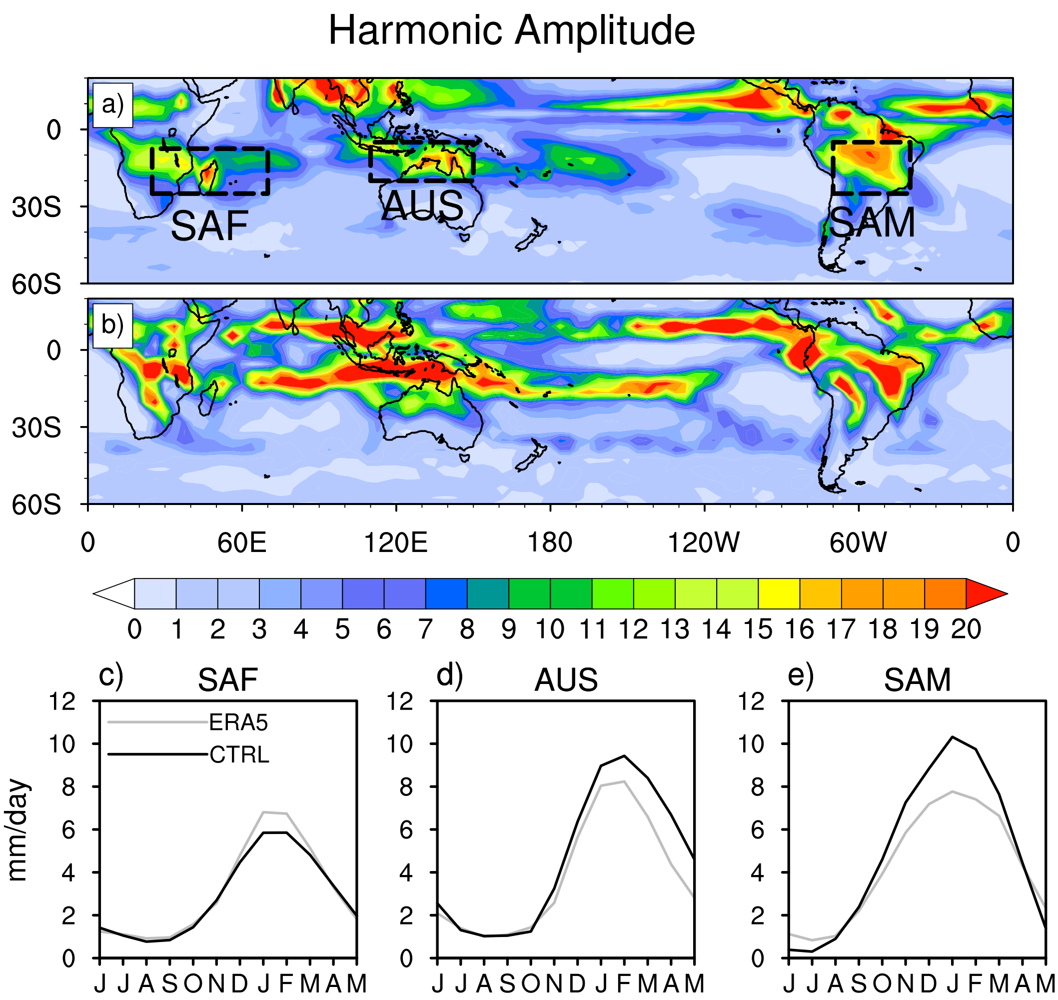

Fig. 3 Amplitude of the 1st harmonic based on ERA5 (a), and the CTRL simulation (b). (d) and (e) show the climatological annual cycle of areal averaged precipitation across the SAFSM, AUSSM and SASM domains (mm/day).

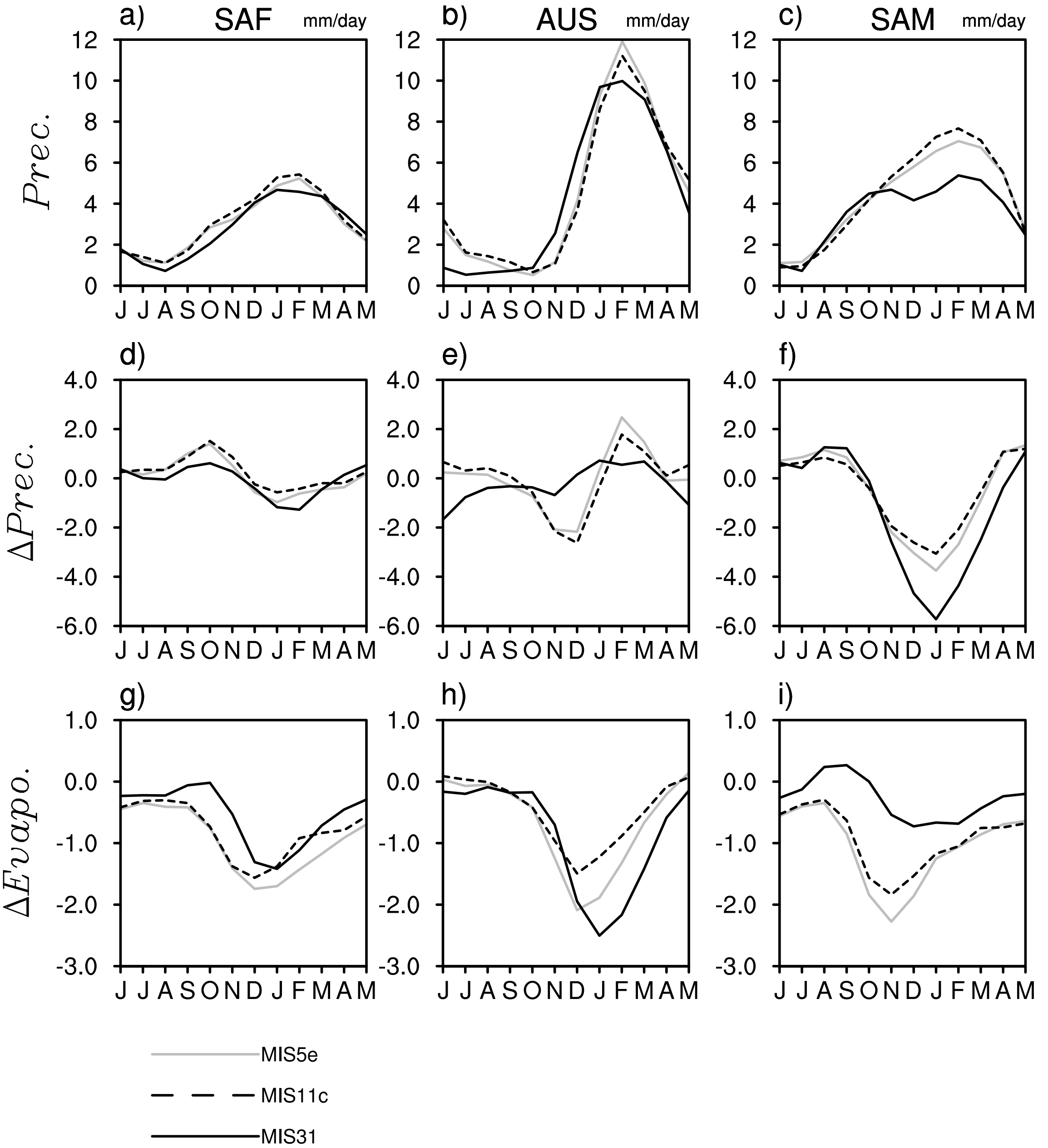

Fig. 4 Climatological annual cycle of precipitation for SAF (a), AUS (b), and SAM (c). (d-e-f) show differences of precipitation ($\Delta Prec$) between the MIS5e, MIS11c, and MIS31 with respect to CTRL conditions. (g-h-i) are the same as (d-e-f) but for evapotranspiration (mm/day, $\Delta Evapo.$).

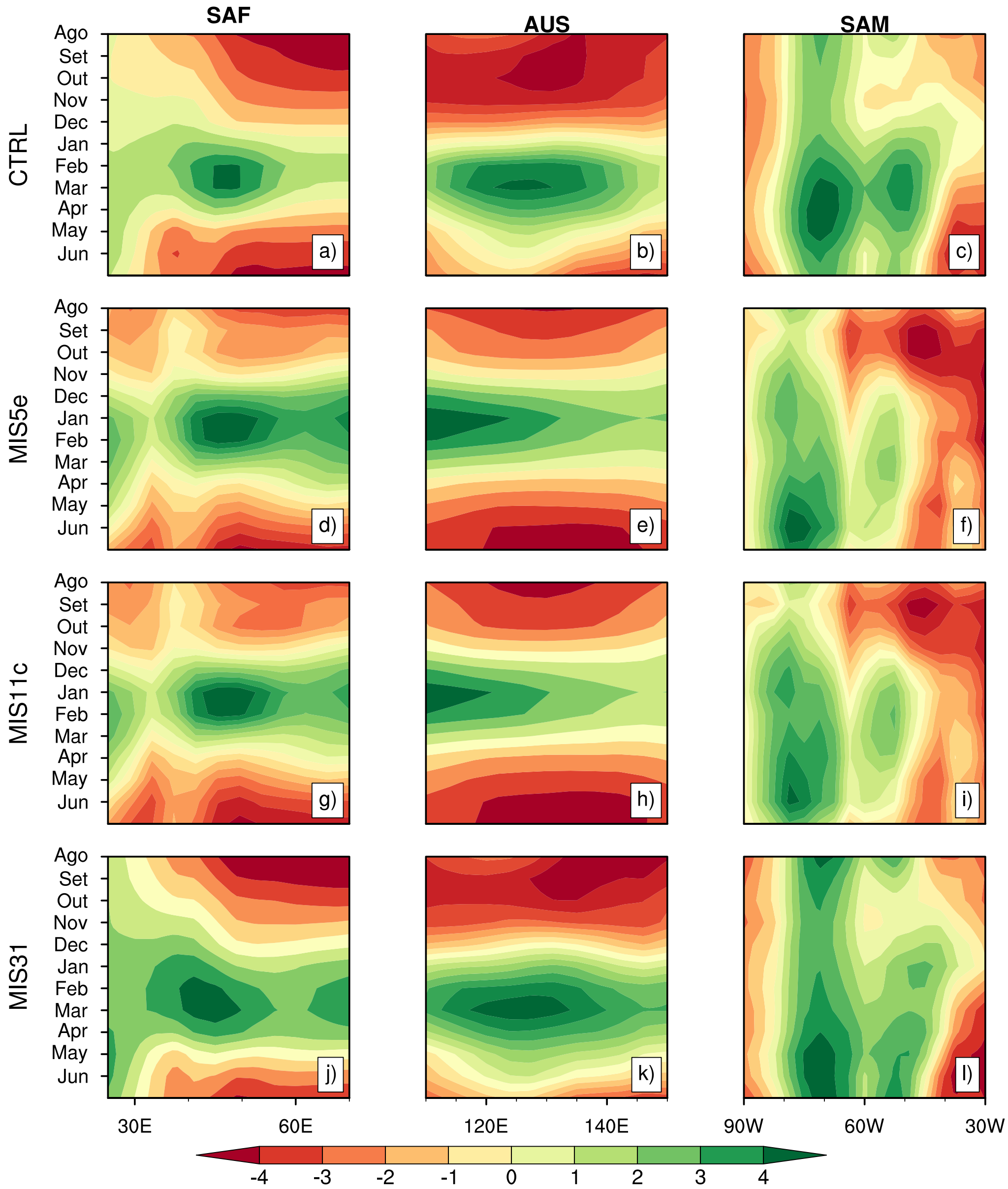

Fig. 5 Longitude-time cross-section of climatological zonal wind (m/s) at 850 hPa averaged between latitudes 7.5°S–25°S (SAF), 5°S-20°S (AUS) and 5°S–25°S (SAM).

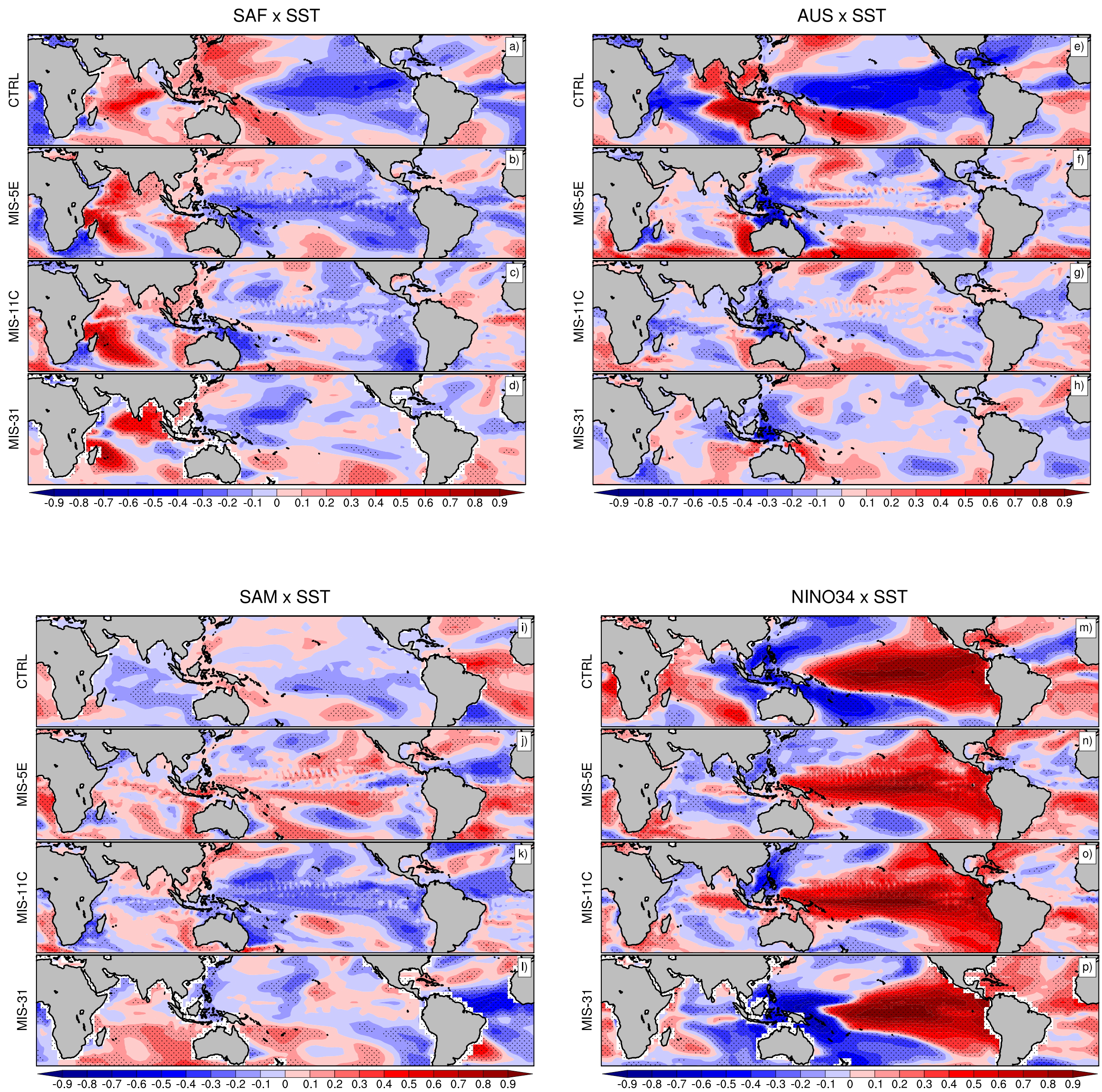

Fig. 6 Correlation coefficient between regional summer monsoons precipitation indices and SST for SAF (a-d), AUS (e-h) and SAM (i-l). (m-p) display the correlation between the Niño 3.4 and SST anomalies. Also shown is the 95% significant areas (dotted grids).

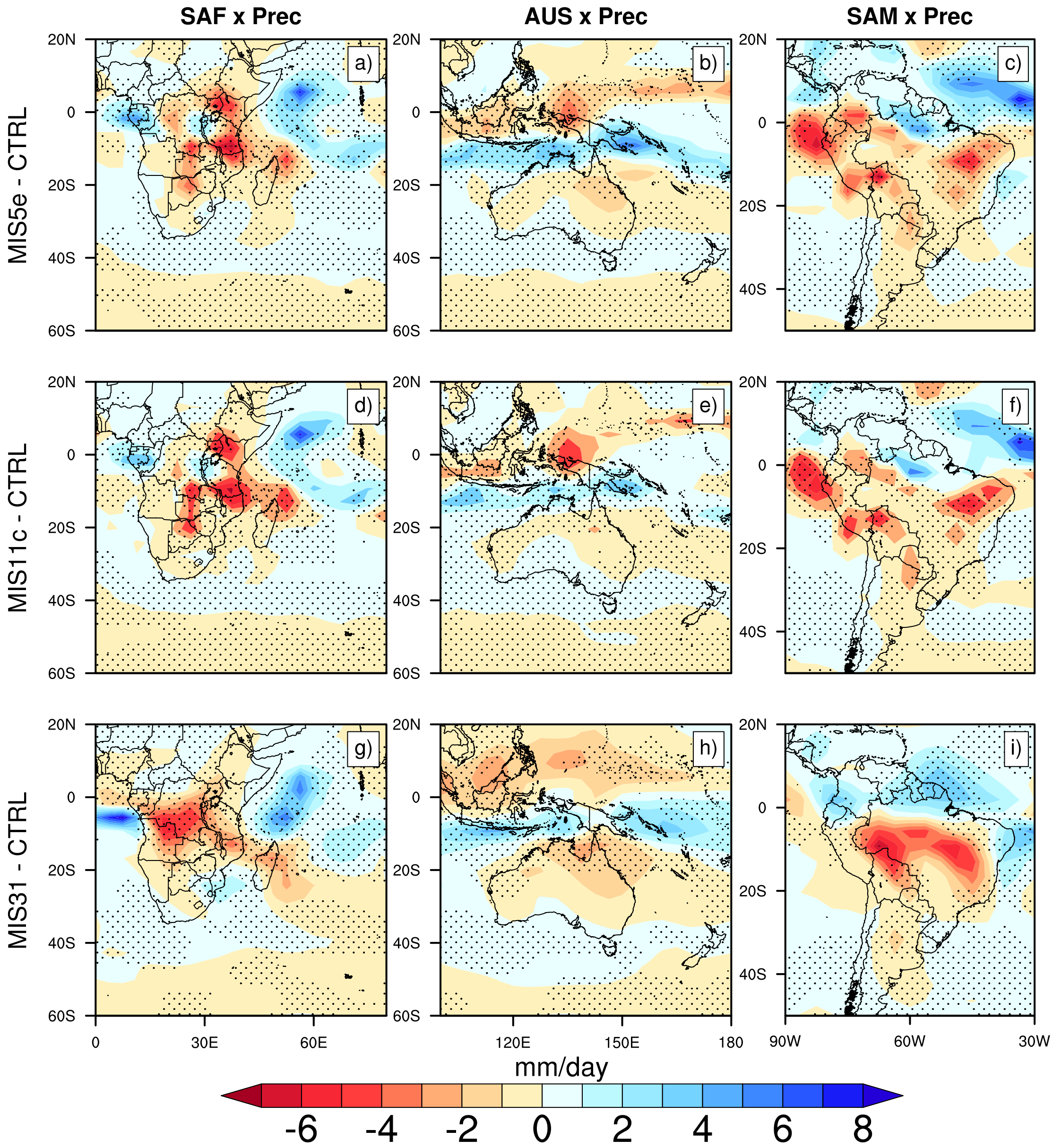

Fig. 7 Precipitation anomalies between MIS5e minus CTRL (a-b-c); MIS11c minus CTRL (d-e-f) and MIS31 minus CTRL (g-h-i). Dots indicate significant correlation between the regional monsoonal vorticity index and precipitation.

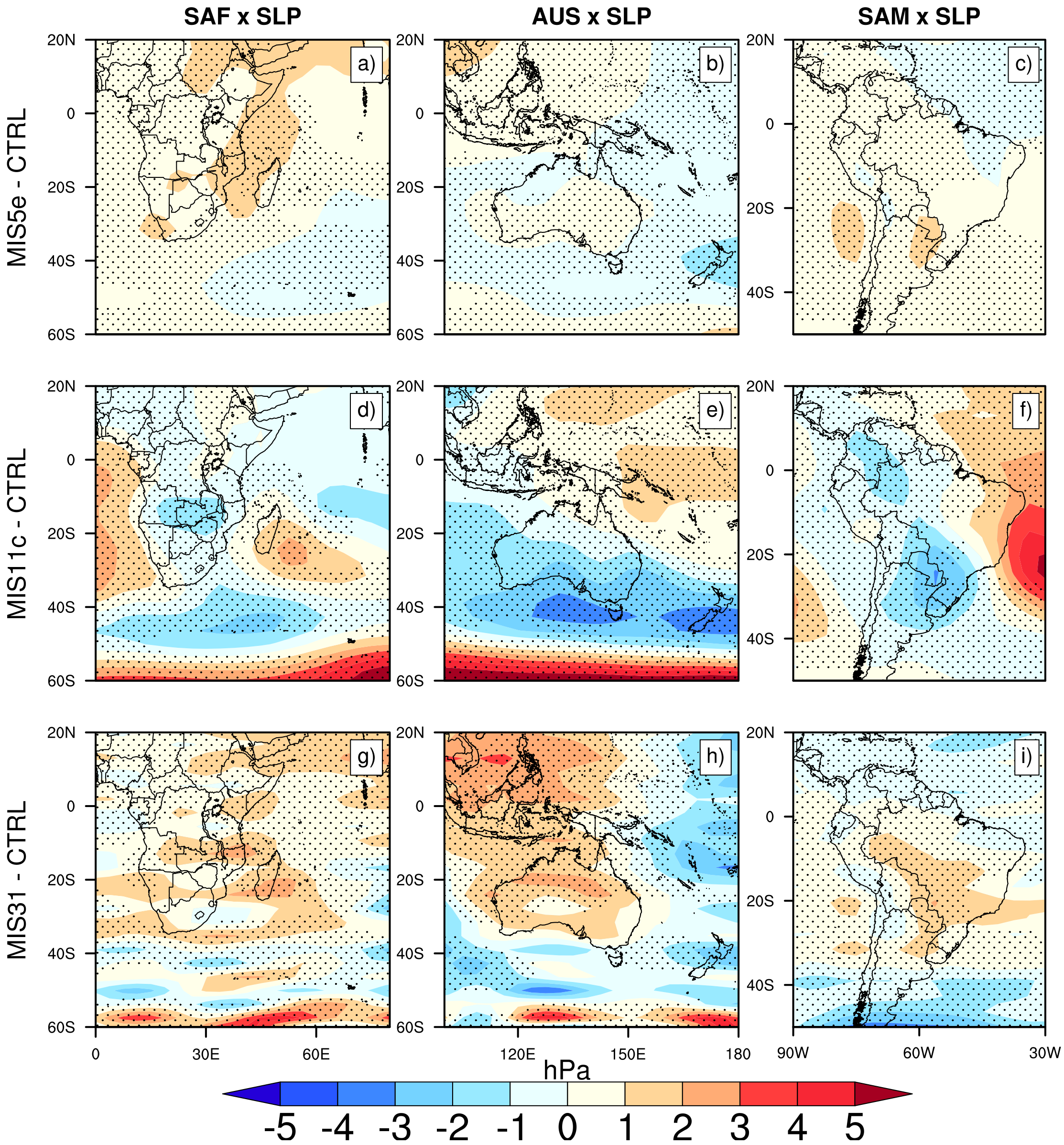

Fig. 8 Same as figure 7 but for SLP.

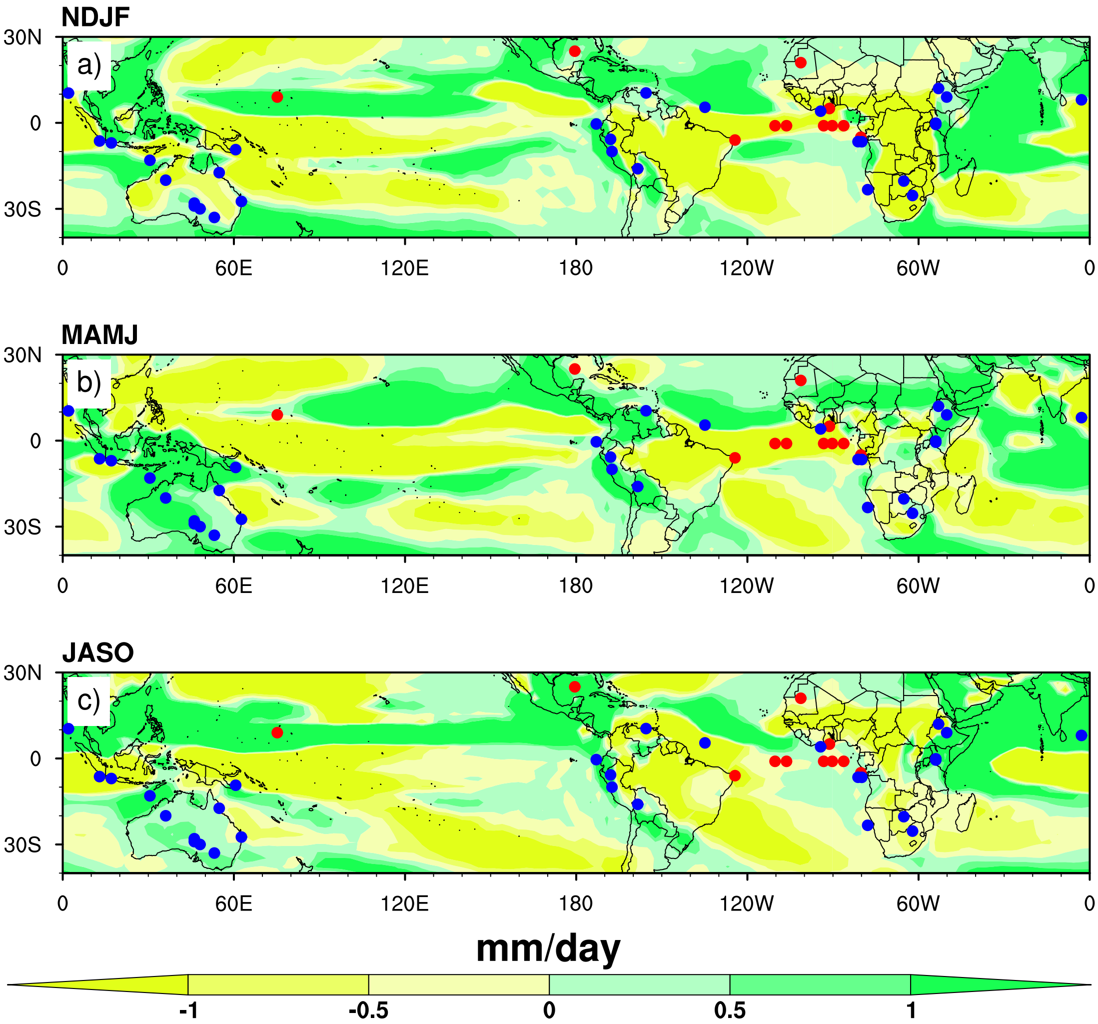

Fig. 9 Map showing precipitation differences between MIS5e and CRTL simulations overlaid by proxy records (wet-blue dots and dry-red dots) during the MIS5e, with respect the present day; for NDJF a), MAMJ b) and JASO c)